# NAVAL POSTGRADUATE SCHOOL

## MONTEREY, CALIFORNIA

# THESIS

**PERFORMANCE AND FLOW REGIMES IN PLANE 2-D DIFFUSERS WITH EXIT CHANNELS AT LOW REYNOLDS NUMBERS**

by

Epameinondas Trivilos

September 2003

Thesis Advisor:                                    Knox T. Millsaps

**Approved for public release; distribution is unlimited.**

THIS PAGE INTENTIONALLY LEFT BLANK

<table>
<tr><td colspan="4" align="center"><strong>REPORT DOCUMENTATION PAGE</strong></td><td colspan="2"><em>Form Approved OMB No. 0704-0188</em></td></tr>
</table>

| | REPORT DOCUMENTATION PAGE | | | *Form Approved OMB No. 0704-0188* | |
|---|---|---|---|---|---|

Public reporting burden for this collection of information is estimated to average 1 hour per response, including the time for reviewing instruction, searching existing data sources, gathering and maintaining the data needed, and completing and reviewing the collection of information. Send comments regarding this burden estimate or any other aspect of this collection of information, including suggestions for reducing this burden, to Washington headquarters Services, Directorate for Information Operations and Reports, 1215 Jefferson Davis Highway, Suite 1204, Arlington, VA 22202-4302, and to the Office of Management and Budget, Paperwork Reduction Project (0704-0188) Washington DC 20503.

| **1. AGENCY USE ONLY** *(Leave blank)* | **2. REPORT DATE** September 2003 | **3. REPORT TYPE AND DATES COVERED** Engineer and Master's Thesis | |
|---|---|---|---|

| **4. TITLE AND SUBTITLE**: Performance and Flow Regimes in Plane 2-D Diffusers with Exit Channels at Low Reynolds Numbers | **5. FUNDING NUMBERS** |
|---|---|
| **6. AUTHOR(S)  Epameinondas Trivilos** | |
| **7. PERFORMING ORGANIZATION NAME(S) AND ADDRESS(ES)** Naval Postgraduate School Monterey, CA  93943-5000 | **8. PERFORMING ORGANIZATION REPORT NUMBER** |
| **9. SPONSORING /MONITORING AGENCY NAME(S) AND ADDRESS(ES)** N/A | **10. SPONSORING/MONITORING AGENCY REPORT NUMBER** |

**11. SUPPLEMENTARY NOTES**  The views expressed in this thesis are those of the author and do not reflect the official policy or position of the Department of Defense or the U.S. Government.

| **12a. DISTRIBUTION / AVAILABILITY STATEMENT** Approved for public release; distribution is unlimited. | **12b. DISTRIBUTION CODE** |
|---|---|

**13.  ABSTRACT** *(maximum 200 words)*

A numerical study on laminar incompressible flows in 2-D straight walled diffusers in the low Reynolds number regime (105-1048) is presented to investigate performance and various flow regimes that might exist. Tail channels are situated downstream the diffusers. Geometries with area ratios AR=1.15 to 5 and non-dimensional lengths of $L/W_1$=1 to 48 are considered. Results are presented in terms of flow regime maps for Reynolds numbers of 105, 210, 314, 420, 629, 1,048 and pressure recovery coefficients maps for Re numbers of 105, 210, 314, 420 and 629. In addition time resolved simulations of impulsively starting flow are considered at Re=210, 314 for 12 geometries on the flow regime map. Four flow regimes can be distinguished depending on diffuser geometry. With increasing divergence angle the flow goes from attached to symmetrically separated to asymmetrically separated and finally to a non 2-D pattern respectively.

| **14. SUBJECT TERMS:** Diffusers, Low Reynolds, Diffuser performance, Diffuser flow regime. | **15. NUMBER OF PAGES** 99 |
|---|---|
| | **16. PRICE CODE** |

| **17. SECURITY CLASSIFICATION OF REPORT** Unclassified | **18. SECURITY CLASSIFICATION OF THIS PAGE** Unclassified | **19. SECURITY CLASSIFICATION OF ABSTRACT** Unclassified | **20. LIMITATION OF ABSTRACT** UL |
|---|---|---|---|

NSN 7540-01-280-5500

Standard Form 298 (Rev. 2-89)
Prescribed by ANSI Std. 239-18

i

THIS PAGE INTENTIONALLY LEFT BLANK

**PERFORMANCE AND FLOW REGIMES IN PLANE 2-D DIFFUSERS WITH EXIT CHANNELS AT LOW REYNOLDS NUMBERS**

Epameinondas Trivilos
Lieutenant, Hellenic Navy
B.S., Hellenic Naval Academy, 1995

Submitted in partial fulfillment of the
requirements for the degree of

**MECHANICAL ENGINEER**

and

**MASTER OF SCIENCE IN MECHANICAL ENGINEERING**

from the

**NAVAL POSTGRADUATE SCHOOL**
**September 2003**

Author:          Epameinondas Trivilos

Approved by:     Knox Millsaps
                 Thesis Advisor

                 Anthony J. Healey
                 Chairman, Department of Mechanical and Astronautical Engineering

iii

THIS PAGE INTENTIONALLY LEFT BLANK

# ABSTRACT

A numerical study on laminar incompressible flows in 2-D straight walled diffusers in the low Reynolds number regime (105-1048) is presented to investigate performance and various flow regimes that might exist. Tail channels are situated downstream the diffusers. Geometries with area ratios AR=1.15 to 5 and non-dimensional lengths of $L/W_1$=1 to 48 are considered. Results are presented in terms of flow regime maps for Reynolds numbers of 105, 210, 314, 420, 629, 1,048 and pressure recovery coefficients maps for Re numbers of 105, 210, 314, 420 and 629. In addition time resolved simulations of impulsively starting flow are considered at Re=210, 314 for 12 geometries on the flow regime map. Four flow regimes can be distinguished depending on diffuser geometry. With increasing divergence angle the flow goes from attached to symmetrically separated to asymmetrically separated and finally to a non 2-D pattern respectively.

THIS PAGE INTENTIONALLY LEFT BLANK

# TABLE OF CONTENTS

# LIST OF FIGURES

# LIST OF TABLES

THIS PAGE INTENTIONALLY LEFT BLANK

# LIST OF SYMBOLS, ACRONYMS, AND/OR ABBREVIATIONS

| Symbols | Description | Units |
|---|---|---|
| AR | Area ratio | [1] |
| AS | Aspect ratio | [1] |
| $C_p$ | Pressure recovery coefficient | [1] |
| $C_{pm}$ | Maximum pressure recovery coefficient | [1] |
| $Cp_{,i}$ | Ideal pressure recovery | [1] |
| F | Similarity velocity profile | [1] |
| G | Normalized velocity profile | [1] |
| L | Diffuser length | [m] |
| $L/W_1$ | Non-dimensional diffuser length | [m] |
| Ma | Mach number | [1] |
| ODE | Ordinary Differential Equation | |
| P | Static pressure | [1] |
| Re | Reynolds number | [1] |
| U | Mean velocity in a cross section | [1] |
| u | r-velocity component in polar coordinates | [m/sec] |
| $u_r, u_\theta, u_\varphi$ | Velocity components in spherical coordinates | [m/sec] |
| v | $\theta$-velocity component in polar coordinates | [m/sec] |
| $u_m$ | Centerline velocity | [m/sec] |
| W | Channel height | [m] |

| Greek symbols | Description | Units |
|---|---|---|
| $\alpha$ | Half diffuser angle | [rad] |
| $\varepsilon$ | Diffuser effectiveness | [1] |
| $\eta$ | Normalized diffuser angle | [1] |
| $\theta$ | Theta coordinate | [rad] |
| $\pi$ | Total pressure ratio | [1] |
| $\rho$ | Density | [$m^2$/sec] |
| $\varphi$ | Phi coordinate | [rad] |

| Subscripts | Description |
|---|---|
| 1 | Inlet |
| 2 | Outlet |

THIS PAGE INTENTIONALLY LEFT BLANK

# ACKNOWLEDGMENTS

THIS PAGE INTENTIONALLY LEFT BLANK

# I.    INTRODUCTION

## A.    OVERVIEW

A diffuser is a common device used in internal flow systems. Such flow systems are encountered in turbomachines between a compressor and a combustor or at the exit of a turbine, duct flows, flow meters, aircraft engine inlets, closed circuit wind tunnels, and pumps. Diffusing passages may also be encountered in small-scale devices such as fluidic actuators and Micro-Electro-Mechanical Systems (MEMS).

The primary purpose of using a diffuser in most of the aforementioned applications is to maximize static pressure recovery while minimizing total pressure loss along the direction of the flow. In other words a diffuser serves as a converter of the flow dynamic head to static pressure. This is achieved by small angle divergent walls, in which the flow is confined, resulting in a certain cross sectional area increase.

Unlike nozzles where the static pressure decreases in the flow direction (favorable pressure gradient), the fluid particle flowing through a diffuser experiences an increasing static pressure (adverse pressure gradient) resulting to a number of fluid dynamic phenomena. These phenomena range from flow separation and unsteadiness to transitory stall and violent flow-excited static pressure fluctuations. Most of these flow situations are very complicated and although they are qualitatively understood they are hard to predict quantitatively.

In Figure1, 2, and 3 the most common and simple diffuser shapes and relevant geometric parameters are shown. However one can have more general shapes of diffusers like the curved ones shown in Fig.4, which depicts diffusing passages in an axial compressor stage.
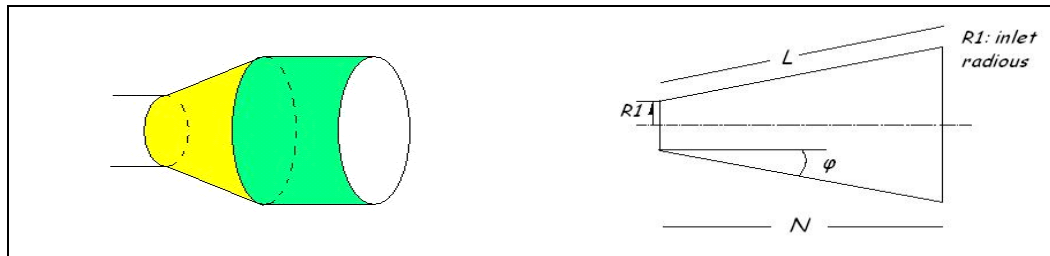


Figure 1.          Conical diffuser
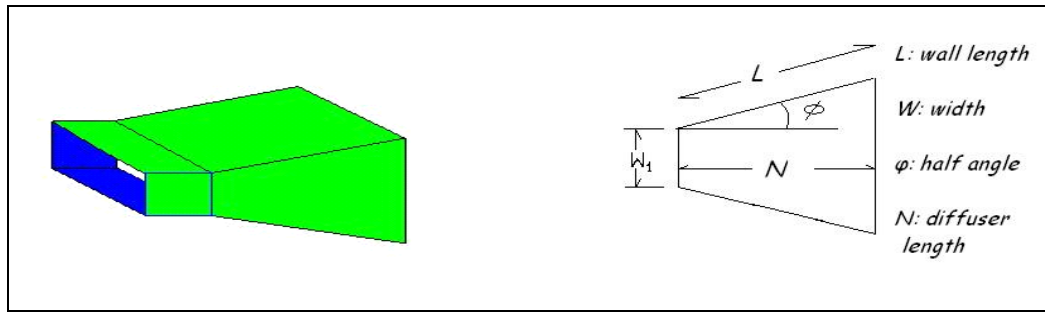
Figure 2.          Rectangular 3-D diffuser
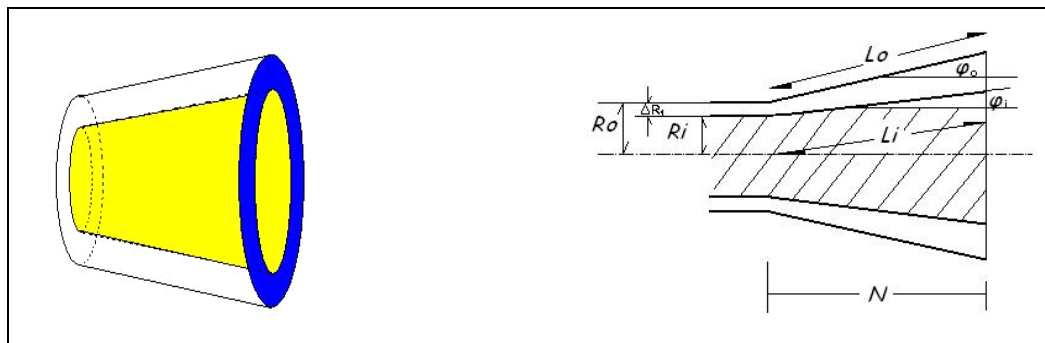


Figure 3.          Annular diffuser
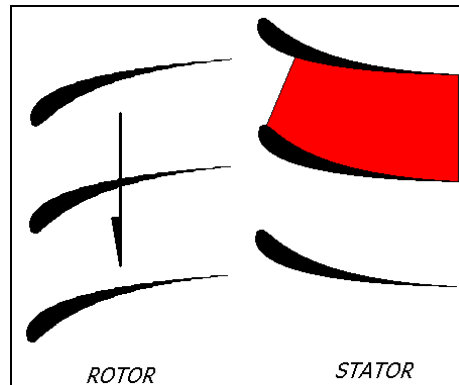


Figure 4.          Stator blades diffuser.

Because of the complexity of the diffuser problem a great number of different variables must be considered in order to study diffuser flows. The parameters driving diffuser flow behavior and performance can be divided in two categories. The first is diffuser geometrical shape parameters. The second is flow parameters.

The geometric parameters are generally described as non-dimensional length L/W$_1$ which is the ratio of the diffuser length to throat width, the area ratio between outlet and inlet cross sections AR, the half angle of divergence θ, the inlet ratio of the radii in the case of annular diffusers or the aspect ratio AS (width to height) in the case of rectangular diffusers, depending on the choice made and the geometry in hand.

The flow parameters are related to the flow conditions in hand. Inlet flow variables such as turbulence intensity, inlet swirl, boundary layer thickness (blockage factor), shape of the velocity profile at the inlet, presence of wakes or stall regions at the inlet, throat Reynolds number, throat Mach number, inlet-outlet flow blockage, other flow devices situated upstream or downstream of the diffuser, are some of the flow parameters driving diffuser performance and behavior.

Typically three factors are used to quantify efficiency and performance of a diffuser. The first is a pressure recovery coefficient $C_p$, defined as the ratio of the difference between exit static pressure $p_{out}$ and inlet static pressure $p_{in}$ to the throat dynamic head and used mostly for subsonic flows:

$$C_p = \frac{p_{out} - p_{in}}{1/2\rho U^2}$$

Where $\rho$ is the density and U is the mass averaged flow velocity. The second factor is a loss coefficient $\pi_d$ defined as the ratio of the outlet to inlet total pressures $P_{Tout}, P_{Tin}$ and used for supersonic flows where the total pressure loss in the diffuser is more significant:

$$\pi_d = \frac{P_{Tout}}{P_{Tin}}$$

The third factor is diffuser effectiveness $\varepsilon$. It is defined as the ratio of measured pressure recovery $C_p$ to ideal inviscid pressure recovery $C_{p,i}$:

$$\varepsilon = \frac{C_p}{C_{p,i}}$$

In general it is desired to optimize diffuser design by maximizing the above factors. High $C_p$ means that the diffuser recovers the greatest amount of static pressure possible from the incoming dynamic head. High $\varepsilon$ means a good static pressure recovery relative to a maximum possible ideal value for inviscid flow through the same diffuser. However there are applications where other characteristics of the flow field are of interest apart from max recovery or effectiveness. It may be needed to have as uniform a flow as possible at the outlet of the diffuser or flow free of pressure oscillations (i.e. combustion flows).

In many cases diffuser performance augmentation takes place by some means of separation control such as wall suction or blowing, vortex generators, vanes, screens, etc. The objective is to reenergize the momentum deficient flow near the diffuser walls such that separation does not take place.

## B.    LITERATURE REVIEW ON SUBSONIC DIFFUSERS

Research work on diffuser flow spans several decades. Gibson G.H. and Eiffel G. reported experimental results as early as 1910 and 1919 respectively [23,24]. More attention was drawn to diffuser flows in the early fifties at the same time with the advent of high-speed flight and the increase in need to have more efficient and reliable internal combustion engines in which the diffuser is an important integral part. As a result high Reynolds number subsonic and supersonic flows were considered in the early experimental investigations. Because this work will consider only subsonic flows, a brief review of prior work in such flows will be presented here. The various parameters and their influence on diffuser performance will be explained. Such prior work on subsonic diffusers can be divided as follows:

1) Experimental/analytical work on steady incompressible flow in diffusers of various geometric shapes. The flow at the diffuser throat has been taken to have an inviscid core with thin turbulent or laminar boundary layers.

2) Experimental/analytical work on unsteady flow though diffusers with throat flow characteristics same as the ones mentioned above in 1.

4

3) Experimental work on improving performance by controlling the diffusing flow separation using various means (vortex generators, wall jets, wall suction, screens or vane insertion, and others).

4) Numerical methods applied to compute diffuser flows.

In 1959, Kline et al [1, 4] reported data on performance and flow regimes for incompressible high Reynolds number flow (Re>70,000) in two dimensional straight wall diffusers. The authors provided and an extensive literature survey. In their experiment they varied diffuser length to inlet height $L/W_1$ from 1.5 to 25 and the area ratios AR from 1.3 to 10. The inlet velocity profiles used had an inviscid core and small turbulent boundary layers close to the walls. The data are correlated in flow regime maps and the following important observations were made: The flow in a diffuser when the throat width, wall length and inlet flow conditions are held constant, while increasing the angle of divergence from zero degrees, can be classified in four distinct regimes:

1) A region of no appreciable stall in which the main flow is almost steady and not separated,

2) A region of large transitory stall in which the flow is unsteady and highly pulsating,

3) A region of fully developed stall on one wall of the diffuser where the flow is steady, and

4) A region in which jet flow emerges from the throat and separation begins just down stream of the throat.

All the above flow regimes were presented in a map shown below in Fig.5. They also discussed if and which of the flow parameters might have the most influence on the above flow regimes. One major characteristic is the independence of the flow regimes on Reynolds number in the range tested above. It is also found that increasing the free stream turbulence intensity has the effect of shifting a-a line of no appreciable stall down. In regard to the effect of aspect ratio AS on flow regimes the data suggested that for aspect ratios above 1:4 there is no appreciable change in the flow regimes.
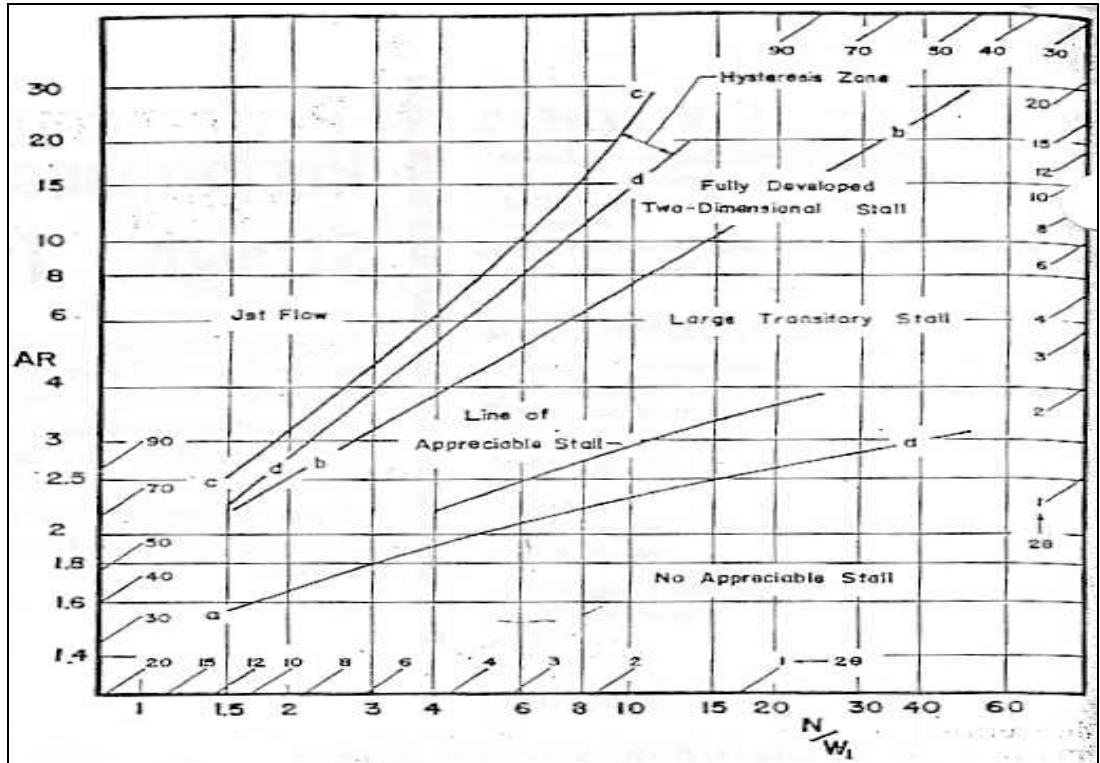
Figure 5.        High Re number diffuser flow regimes map (Adapted from [2]).

In a 1961 paper Waitman et al ([2]) reported an experimental study on the influence of inlet boundary layer thickness in the performance of two-dimensional subsonic diffusers. Several diffusers were tested spanning inlet lengths to heights from 8.0 to 48.0, total divergence angles from 2.5 to 40 degrees. Inlet boundary layers were turbulent and varied from extremely thin to fully developed turbulent channel flow. Low Mach number (<0.2), high throat Reynolds number (Re>10,000) were used. Flow obstructions upstream of the diffuser throat were also used for brief investigation on the effects of their wakes on performance. It was found that pressure recovery is a strong function of inlet boundary layer thickness, decreasing with increased thickness. Turbulence intensity was found to increase pressure recovery as intensity increased. The flow regimes chart given in ref. [1] was altered by small degree in the sense that stalls appeared in smaller value of angle of divergence as boundary layer thickened at the inlet.

In 1965 [3] Sorvan and Klomp gave an extensive experimental investigation of pressure recovery on a large number of annular, low subsonic diffusers (Ma<0.3). Also

6

data for rectangular and conical diffusers from previous studies, like [1], [2], were gathered and used for evaluation of performance characteristics for all three types of geometries. The study showed a significant degree of similarity on performance among the three types of diffusers, if $N/W_1$, $N/R_1$, $L/\Delta R_1$ are taken as the non-dimensional length parameter for rectangular, conical, annular units respectively. The concept of area blockage was shown to correlate the effect of inlet boundary layer thickness on pressure recovery for all three types of diffusers. Area blockage occurs in internal flow sytems because of the non-uniformities in velocity over the cross section of the systems. The idea of "inefficient" versus "insufficient" diffusion is introduced; the first describing viscous effects on diffuser effectiveness while the second implying deviations from ideal one-dimensional inviscid flow due to velocity profile non-uniformities. It is shown that the reduction in pressure recovery due to boundary layer thickening is primarily the result of "insufficient" rather than "inefficient" diffusion.

Wolf and Johnston [5] investigated the effect of non-uniform inlet velocity profiles experimentally. A two-dimensional rectangular diffuser is chosen and the inlet velocity profile is changed to include wakes, non-uniform shear and jet type flows. The most important of their results is the increase in pressure recovery for several geometries when a wake is present in the inlet profile. However all other types of inlet non-uniformities decrease recovery. Wake non-uniformities are amplified downstream the diffuser. Also diffuser flow regimes are shown to depend on the relative location of the low velocity fluid at the inlet profile. If the low velocity fluid is near to one inlet wall, separation tends to appear on that wall.

McMillan and Johnston [6], [7] treat a low aspect ratio (AS=0.1) two-dimensional diffuser with fully developed turbulent inlet flow. The importance of AS alone is investigated experimentally in the Reynolds number range from 20,000 to 70,000. The specific feature of this type of diffuser is the close proximity of the parallel walls and the effect that this might have on diffusion, since the "presence" of these walls through viscosity can be felt in the core flow. The results show that flow regimes are more dependent upon inlet conditions compared to high aspect ratio diffusers. Regime transitions depend strongly on inlet Re number as well as the diffuser geometry. On the contrary experience with high aspect ratio diffusers shows that flow regime depends

primarily on diffuser geometry and only slightly on inlet flow conditions and Re number. Pressure recovery was found to increase with increasing Reynolds number for the low aspect ratio diffuser. Losses of total pressure along the diffuser are comparable to those of a straight channel of the same length as the diffuser.

Runstadler and Dolan [8, 9] investigate high subsonic flow in two-dimensional diffusers. They employ geometries of different lengths, aspect ratios from 0.25 to 5, inlet Ma numbers from 0.2 to 1.0; blockage factors from 0.02 to 0.12.From the collected experimental data performance maps are constructed while aspect ratio, Ma number, blockage and Re number being held constant. The diffuser performance maps for compressible flow are significantly different from the maps taken for incompressible flows. Higher blockage reduces the pressure recovery. Inlet Ma was shown to have a very mild increasing effect on recovery up until chocking, beyond witch the recovery deteriorates rapidly. Increasing Reynolds number (varied from 170,000 to 580,000) produces an increase in pressure recovery.

Dighe and McDonald [10] investigated the effect of aspect ratio on plane-wall diffuser performance and flow regimes for Re numbers in the range 3,000<Re<28,000 and with laminar boundary layers at the diffuser throat. They employ twelve diffuser geometries with aspect ratios 0.21<AS<2.65 and. All diffusers used had constant length $N/W_1$=18 and total divergence 4$^o$ half angle. The results show that Re number has a profound effect on pressure recovery for all aspect ratios tested, increasing Re number from 3,000 to 20,000 increases recovery from 0.4 to 0.75 at constant aspect ratio . Even though diffuser geometries are chosen to be in the unstalled flow regime, when the throat Re number was low 3000<Re<5000, flow regime changed: This is an indication that for lower Reynolds number flows Reynolds number is a controlling flow regime parameter. Jet flow was observed for low aspect ratio diffusers (AS<0.94), while two dimensional stall was exhibited in diffusers with AS>0.94. Above Re=5000 none of the diffusers investigated in this study exhibited stall.

Stenning [11], Smith [12], and Kwong [13] investigated unsteady diffusers flows in a Re number range of 3,000 to 20,000. They conclude that amplification of inlet mean flow oscillations in the diffuser take place when throat Re number is in the region of 3000

to 6000, self-excited low frequency flow oscillations occur in the transitory stall regime (for Re numbers higher than 12,000-15,000) and that an amplification of such oscillations happens when inlet disturbances are present with periods 0.5 $T_m$ to $T_m$, were $T_m$ is the mean oscillation period of the stall regions from one wall of the diffuser to the other.

Various methods can be used to enhance performance and /or outlet flow stability and uniformity. The simplest ways employ devices like vortex generators, vanes or screens, calling them passive separation control. Wall suction to take away the low momentum fluid near the wall or blowing to add momentum can be employed. These methods are called active separation control. The general idea used in all methods is to reenergize the boundary layer that forms on the diffuser walls, thus preventing low momentum fluid from separating due to the adverse pressure gradient. It can not be said that one method is more successful over the other because depending on requirements of the design one might exploit advantages of a specific method that are not present in others. See references [14], [15], [16] on diffuser performance augmentation by flow separation control.

In the recent years some effort has been done to compute diffuser flow fields. References [17], [18], [19], [20] are papers devoted in investigating diffuser flows computationally. Successful computations at high Re numbers (where modeling of turbulence is needed) are feasible if the flow inside the diffuser is not separated. That means very low diffusion angles. For separated flows only laminar very low Re (<114) number computations are shown to be feasible [18].

In summary most of the work reported on subsonic diffuser flows is experimental for medium to high Reynolds numbers (>2,000). This work has identified the parameters and the extent each parameter affects diffuser performance and flow regimes. It was shown that geometric variables like AR, AS, $L/W_1$ and flow related variables like Re, Ma, throat boundary layer thickness and turbulence intensity affect diffuser behavior in various degrees mentioned in the preceding paragraphs. The results presented in terms of flow regime and pressure recovery coefficient maps are used to design optimum and efficient diffusers operating in the high Reynolds number range. However little work is reported for diffuser flows in the Re number range below 2,000. In this Reynolds number

range the optimum characteristics of the diffusers have not been extensively investigated. In addition the effect of geometric and flow parameters on diffuser behavior is not extensively studied.

## C.     OBJECTIVES AND SCOPE OF PRESENT WORK

The objectives of this study were:

1) Validate the commercial computational fluid dynamics (CFD) code CFD-ACE+ against a known analytical solution of the 2-D Navier-Stokes equations for straight plane diffuser flows.

2) Investigate different types of flow regimes that might be encountered in a straight plane diffuser with a parallel channel at both inlet and exit while varying the inlet Re number in the range 105-1048 and the geometry of the diffuser in the range of 1.15-5 for the AR and 1-48 for the $L/W_1$. For high Re flows, increasing diffusion angle (all other geometric parameters held constant), the flow undergoes various configurations called flow regimes [1]. In this work a parallel attempt is made but for low Re number fully developed flows and by purely computational means.

3) Determine optimum performance characteristics in terms of maximum static pressure recovery coefficient for the same diffuser geometries and Re number range mentioned in 2 above.

## D.     ORGANIZATION

Chapter II presents a brief description of numerical methods and features of the software package used in this work.

Chapter III discuses exact solutions of the Navier-Stokes equations for Jeffery-Hamel flows in a 2-D diffuser and the accuracy of the software against these solutions.

Chapter IV describes the numerical solution of the Navier-Stokes equations for several diffuser-outlet channel configurations and Re numbers in the 50-1048 interval using the commercial CFD-ACE+ code. The results are correlated in flow regimes and pressure coefficient performance maps.

Chapter V presents the time resolved numerical calculations done in CFD-ACE+ for Re=320, 210 and several diffuser geometries in the two most important flow regimes found in chapter IV.

Chapter VI concludes.

THIS PAGE INTENTIONALLY LEFT BLANK

# II. OVERVIEW OF CFD-ACE+ AND THE SPECIFIC FEATURES OF THE PROGRAM USED IN THIS STUDY

## A. GENERAL DESCRIPTION

The commercial program CFD-ACE+ is a solver that utilizes a finite volume pressure correction based method to solve the conservation equations of mass, momentum and energy. It provides the user three graphical user interfaces (GUI's) namely a preprocessor CFD-GEOM for geometry creation, a processor CFD-ACEU which is the actual solver of the descretized equations and a post processor CFD-VIEW for viewing and processing the results.

## B. NUMERICAL METHODS

### 1. Discretization Schemes

The software provides several different schemes for discretizing the partial differential equations in space and time. Throughout this study the second order scheme will be used for spatial discretization and the Crank-Nicholson scheme for time derivative discretization. The resulting finite difference equations (FDE) are nonlinear algebraic equations formed for each computational shell in the following form:

$$(\alpha_p - S_p)\phi_P = \sum_{nb} a_{nb}\phi_{nb} + S_U$$

Where, $\phi$ is the dependent variable and $\alpha$ the non-linear coefficients. An iterative method is employed to solve the set of the resulting system of non-linear algebraic equations. To formulate an equation for the unknown variable pressure the continuity is used by adopting the SIMPLEC algorithm. For further information on the code the reader is referred to the CFD-ACEU user manual and the additional references therein [22]. Convergence is achieved if the residuals of the dependent variables (pressure, u velocity and v velocity in this study) drop several orders of magnitude (>5) and the continuity equation is satisfied by at least six orders of magnitude after a number of iterations has been performed. Note that from this point on the residual drop and the continuity equation satisfaction with the number of iterations, will be referred to as "residual history" and "mass flow summary" respectively.

13

## 2.    Boundary Conditions

A number of options on boundary conditions are available to the user. Indicated here are the boundary conditions that will be used in this study:

1) Specification of u velocity profiles or uniform total pressure at the computational domain inlet.

2) Static pressure at the computational domain outlet.

3) No slip no penetration conditions at the walls.

## 3.    Grid Generation

The software allows structured and unstructured grid generation. In this work the structured grid is used. For further information about the meaning of each type of grid the reader is referred to the manual. Throughout this study computational shell aspect ratio and skew ness are kept to a minimum. The maximum shell aspect ratio is kept under 8 and the smallest angle in any one shell is kept under $70^{\circ}$.
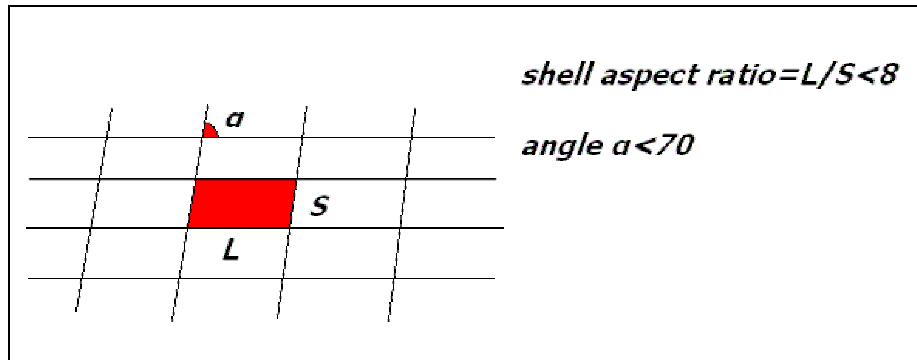


Figure 6.    Computational shell characteristics.

## C.    SPECIFIC CFD-ACEU SETTINGS USED IN THIS STUDY

In this thesis only the "flow" module of the solver will be used since the flow is assumed isothermal and the energy equation need not be solved. Inlet parabolic velocity boundary conditions will be imported as data files after they are generated in MATLAB. Relaxation for the pressure correction equation and velocity variables of 0.1-0.2 and 0.05-0.09 respectively will be used.

# III. ANALYTICAL AND NUMERICAL SOLUTION OF THE NAVIER-STOKES EQUATIONS IN A 2-D DIFFUSER FOR JEFFERY-HAMEL FLOWS

## A. PURPOSE

The Jeffery-Hamel hydrodynamic flow problem in a plane diffuser is a well-known exact analytical solution of the two-dimensional steady incompressible Navier-Stokes equations [21]. In this study the accuracy of the CFD software (used later in the study) will be checked against the analytical solution and it will be shown that the multiplicity of solutions predicted analytically is also observed in the direct numerical solution of the Navier-Stokes equations for flows computed in this study.

## B. ANALYTICAL FORMULATION AND SOLUTION OF THE PROBLEM

### 1. Formulation of the Problem

The hydrodynamic problem is described from the continuity and the Navier-Stokes equations written in polar coordinates form as:

$$\frac{\partial(ru)}{\partial r} + \frac{\partial v}{\partial \theta} = 0 \tag{1}$$

$$u\frac{\partial u}{\partial r} + \frac{v}{r}\frac{\partial u}{\partial \theta} - \frac{v^2}{r} = -\frac{1}{\rho}\frac{\partial p}{\partial r} + \nu(\nabla^2 u - \frac{2}{r^2}\frac{\partial v}{\partial \theta} - \frac{u}{r^2})$$

$$u\frac{\partial v}{\partial r} + \frac{v}{r}\frac{\partial v}{\partial \theta} + \frac{uv}{r} = -\frac{1}{\rho r}\frac{\partial p}{\partial \theta} + \nu(\nabla^2 v + \frac{2}{r^2}\frac{\partial u}{\partial \theta} - \frac{v}{r^2}) \tag{2}$$

The coordinate system is given below:
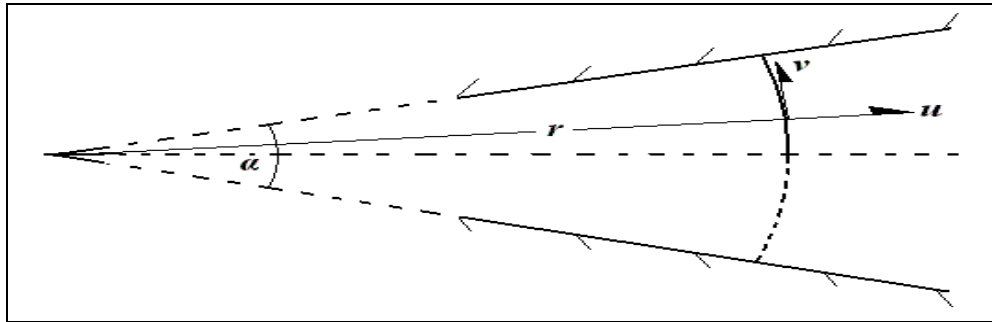


Figure 7.        Diagram of the 2-D diverging channel with the line source at the origin.

If the flow is assumed to be purely radial emerging from a line source that is if $u = u(r, \theta), v = 0$ from continuity (1),

$$\frac{\partial(ru)}{\partial r} = 0 \quad \Rightarrow \quad ru = fnc(\theta) \quad \Rightarrow \quad u = \frac{F(\theta)}{r} \tag{3}$$

Substituting $u = u(r, \theta), v = 0$ back in the momentum equations (2) we get,

$$\begin{cases} u\dfrac{\partial u}{\partial r} = -\dfrac{1}{\rho}\dfrac{\partial p}{\partial r} + v\left[\dfrac{\partial^2 u}{\partial r^2} + \dfrac{1}{r}\dfrac{\partial u}{\partial r} - \dfrac{u}{r^2} + \dfrac{1}{r^2}\dfrac{\partial^2 u}{\partial \theta^2}\right] \\[4mm] 0 = -\dfrac{1}{\rho r}\dfrac{\partial p}{\partial \theta} + \dfrac{2v}{r^2}\dfrac{\partial u}{\partial \theta} \end{cases} \tag{4}$$

From (3) calculate all derivatives in (4) with respect to F:

$$\frac{\partial u}{\partial r} = -\frac{F}{r^2}, \ \frac{\partial u}{\partial \theta} = -\frac{F'}{r}, \ \frac{\partial^2 u}{\partial r^2} = \frac{2F}{r^3}, \ \frac{\partial^2 u}{\partial \theta^2} = \frac{F''}{r} \tag{5}$$

Substitute in (4) to get

$$\begin{cases} \dfrac{\partial p}{\partial r} = \dfrac{\rho F^2}{r^3} + \dfrac{\rho F''}{r^3} \\[4mm] \dfrac{\partial p}{\partial \theta} = \dfrac{2\mu F'}{r^3} \end{cases} \tag{6}$$

Eliminate pressure

$$\left.\begin{array}{l} \dfrac{\partial p}{\partial r} = \dfrac{\rho F^2}{r^3} + \dfrac{\rho F''}{r^3} \\[4mm] \dfrac{\partial p}{\partial \theta} = \dfrac{2\mu F'}{r^3} \end{array}\right\} \Rightarrow \mu F''' + 2\rho FF' + 4\mu F' = 0 \Rightarrow \tag{7}$$

$$F''' + \frac{2}{v}FF' + 4F' = 0 \tag{8}$$

Where: F is the similarity velocity profile. The boundary conditions in terms of the new function F used to solve the third order ode become:

$$F(\pm\alpha) = 0 \tag{9}$$

$$F'(0) = 0 \tag{10}$$

16

If equation (3) is normalized by the value of the velocity profile at $\theta=0$, $F(0)$ and $\theta$ by the max half angle, $a$ of any given diffuser, they take the following form:

$$u(r,0)=u_m=\frac{F(0)}{r} \tag{11}$$

$$G(\theta)=\frac{F(\theta)}{F(0)}, \ \eta=\frac{\theta}{a} \tag{12}$$

$$F(0)\frac{d^3G}{a^3d\eta^3}+\frac{2}{v}F(0)G\frac{dG}{ad\eta}+4F(0)\frac{dG}{ad\eta}=0 \Rightarrow \tag{13}$$

$$\frac{d^3G}{d\eta^3}+\frac{2F(0)a^2}{v}G\frac{dG}{d\eta}+4a^2\frac{dG}{d\eta}=0 \tag{14}$$

Or

$$G'''+2a\,\mathrm{Re}\,GG'+4a^2G'=0 \tag{15}$$

Where G is the normalized similarity profile and Re is a Reynolds number

$$\mathrm{Re}=\frac{u_m ra}{v} \tag{16}$$

Note for small channel angles α, $ra$ is approximately equal to the channel half height. The boundary conditions are transformed to:

$$G(\pm1)=0 \tag{17}$$

$$G'(0)=0 \tag{18}$$

$$G(0)=1 \tag{19}$$

This non-linear third order ode along with the boundary conditions is solved for the invariant velocity profile $G(\eta)$, the resulting velocity field is found as:

17

$$u(r,\theta)=\frac{F(\theta)}{r}=\frac{F(0)G(\eta)}{r}=u_m G(\theta/a)=\mathrm{Re}\frac{v}{ar}G(\theta/a) \tag{20}$$

Also the pressure field can be found as follows:

$$\frac{\partial p}{\partial \theta}=\frac{2\mu F(0)G'}{r^2}\Rightarrow\frac{\partial p(r,\eta)}{\partial \eta}=\frac{2\mu F(0)G'}{r^2} \tag{21}$$

Integrating once with respect to $\theta$ or $\eta$,

$$p(r,\eta)=\frac{2\mu F(0)}{r^2}G(\eta)+c(r)$$

Differentiating with respect to r,

$$\frac{\partial p}{\partial r}=\frac{-4\mu F(0)}{r^3}G(\eta)+c'(r) \tag{22}$$

The second momentum equation solved for the pressure gradient gives:

$$\frac{\partial p}{\partial r}=\frac{\rho F^2}{r^3}+\frac{\mu F''}{r^3}\Rightarrow\frac{\partial p(r,\eta)}{\partial r}=\frac{\rho F(0)^2 G^2}{r^3}+\frac{\mu F(0)G''}{a^2 r^3} \tag{23}$$

Equating the above last two equations and solving for the constant $c(r)$ we get:

$$\frac{-4\mu F(0)}{r^3}G(\eta)+c'(r)=\frac{\rho F(0)^2 G^2}{r^3}+\frac{\mu F(0)G''}{a^2 r^3}\Rightarrow \tag{24}$$

$$c'(r)=\frac{\mu F(0)}{a^2 r^3}\left[G''+\frac{a^2 F(0)}{v}G^2+4a^2 G\right]\Rightarrow$$

$$c'(r)=\frac{\mu F(0)}{a^2 r^3}\left[\underbrace{G''+a\,\mathrm{Re}\,G^2+4a^2 G}_{G''(1)}\right]\Rightarrow$$

$$c(r)=-\frac{\mu F(0)}{2a^2 r^2}G''(1)+c_1 \tag{25}$$

Thus the pressure field is given by:

18

$$p(r,\eta) = \frac{2\mu F(0)}{r^2} G(\eta) - \frac{\mu F(0)}{2a^2 r^2} G''(1) + c_1 \Rightarrow$$

$$p(r,\eta) = \frac{\mu F(0)}{2a^2 r^2} \left[ 4a^2 G(\eta) - G''(1) \right] + c_1 \tag{26}$$

But,

$$\frac{\mu F(0)}{2a^2 r^2} = \frac{\mu}{2a^2 F(0)} u_m^2 = \frac{\nu}{2a^2 F(0)} \rho u_m^2 = \frac{1}{2} \rho u_m^2 \frac{1}{a\,\mathrm{Re}}$$

And if

$$r \to \infty \Rightarrow p(r,\eta) \to c_1 = p_\infty,$$

This means pressure at infinity becomes uniform i.e. the diffuser is very long. Thus,

$$p(r,\eta) - p_\infty = \frac{1}{2} \rho u_m^2 \frac{1}{a\,\mathrm{Re}} \left[ 4a^2 G(\eta) - G''(1) \right] \Rightarrow$$

$$C_p = \frac{p_\infty - p(r,\eta)}{\frac{1}{2} \rho u_m^2} = \frac{1}{a\,\mathrm{Re}} \left[ G''(1) - 4a^2 G(\eta) \right] \tag{27}$$

This is the pressure coefficient that specifies the recovery in static pressure as a function of $r, \eta$.

## 2.    Solution of the Problem

The nonlinear equation (15) will be solved in MATLAB using the build in RUNGE-KUTTA 45 algorithm for ordinary differential equations. Because of the accuracy and robustness of this scheme the solution can be regarded close to an exact analytical solution. The programming specifics are given in Appendix.A. Here the results are presented in the form of velocity profiles for both nozzles and diffusers.
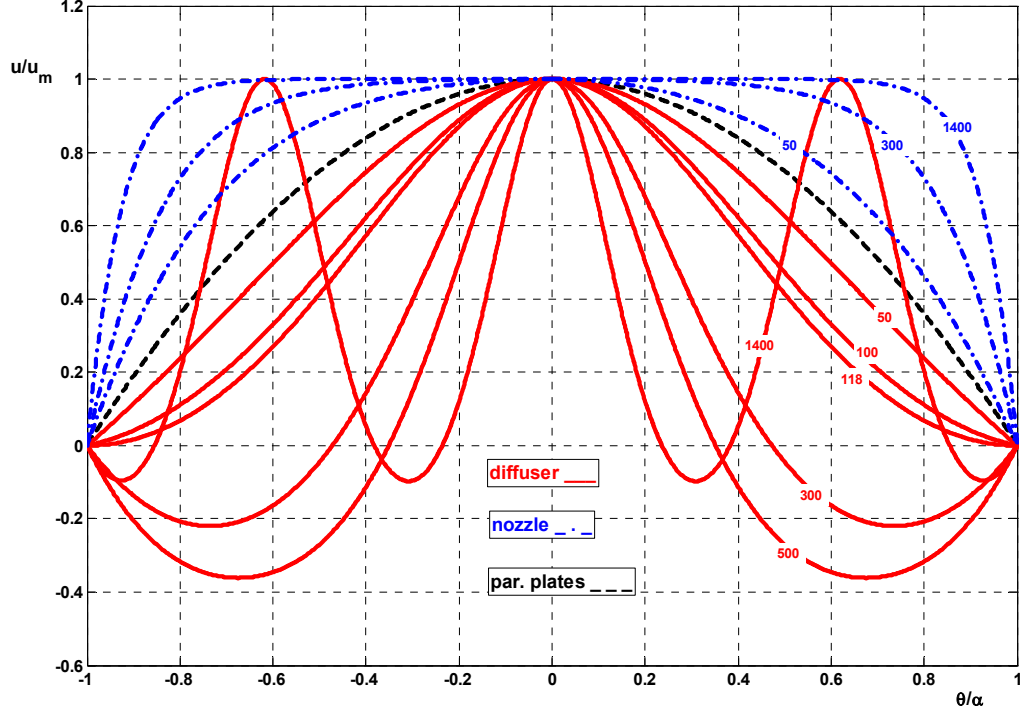
Figure 8.        Velocity profiles for various Reynolds numbers in converging, parallel and diverging channels.

It is seen in Figure 8 that multiple solutions are possible depending on the Reynolds number. Both symmetric and asymmetric velocity profiles are possible in a diffuser. The elliptic integral solution [21] of the non-linear differential equation (15) predicts a separation criterion of $\alpha \, \mathrm{Re} \geq 10.31$. For a five degree half angle divergent walls this means that separation is possible if $\mathrm{Re} > 118$.

## C.      NUMERICAL FORMULATION AND SOLUTION OF THE PROBLEM IN CFD-ACE+.

### 1.      Formulation of the Problem

The software CFD-ACE must be supplied with a specific bounded geometry. Here we choose a diffuser of half angle 5 degrees with the spatial dimensions shown in the following figure in [m]:

20

Figure 9.        Diffuser geometry and dimensions.

The area ratio is approximately 3 and the non-dimensional length 23. This gives a five-degree half angle. The objective is to compute the flow field in CFD-ACE for boundary conditions taken the same as the ones used in the analytical solution. The compute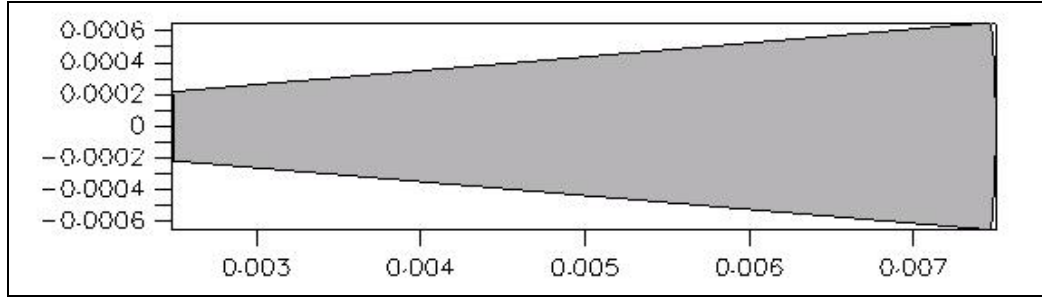d flow field will be checked against the analytical field at two stations for the velocity profiles (0.004 m and 0.007 m) and the centerline for the static pressure distribution. A 300X120 grid and air as a medium will be used in the numerical solution. The Reynolds number will be chosen to be Re=100/0.08726=1146, a value which gives a dimensionless profile approaching separation as shown in Figure 8.

The dimensional velocity and pressure profiles needed for boundary conditions are formulated in MATLAB and for the inlet are given graphically in Figure 10. From the definition of the Re and the velocity profiles at the inlet and outlet of the diffuser we get:
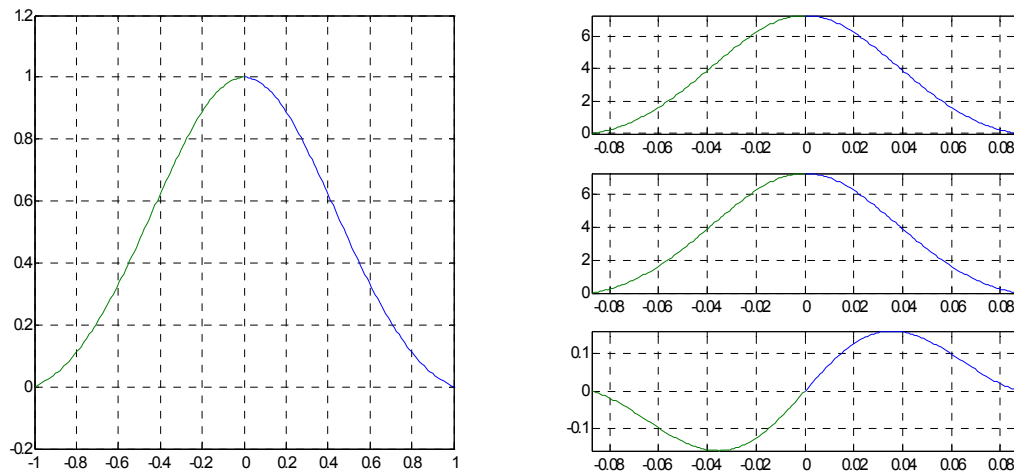


Figure 10.        Velocity profiles at the inlet. On the left non-dimensional, right top dimensional and right middle and bottom decomposed to dimensional x and y components [m/sec].

## 2. Solution of the Problem

The solution of ACE+ is visualized in CFD-VIEW. Results are presented in the forms of velocity contours streamline contours and static pressure contours, in Fig.9, 10, 11 respectively.
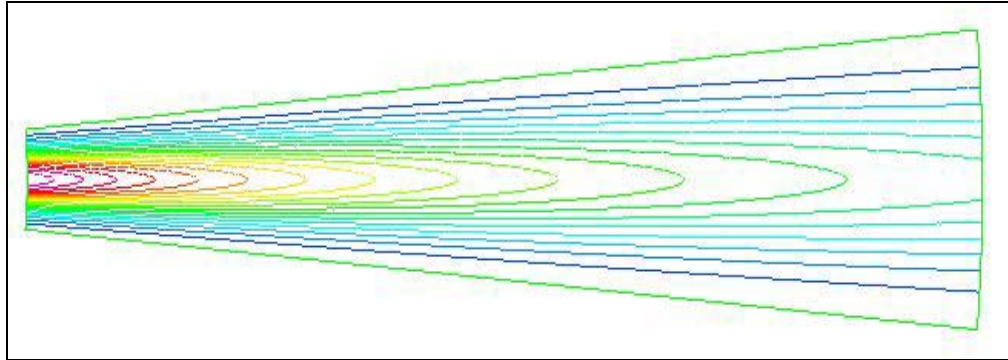


Figure 11.        Velocity contours.
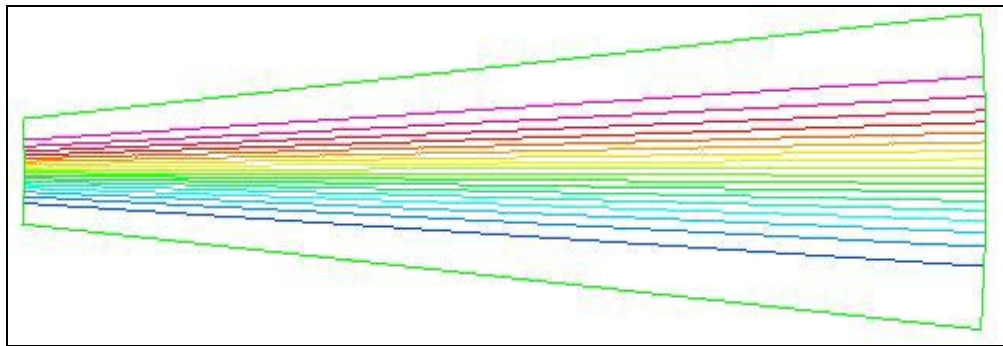


Figure 12.        Streamline contours.
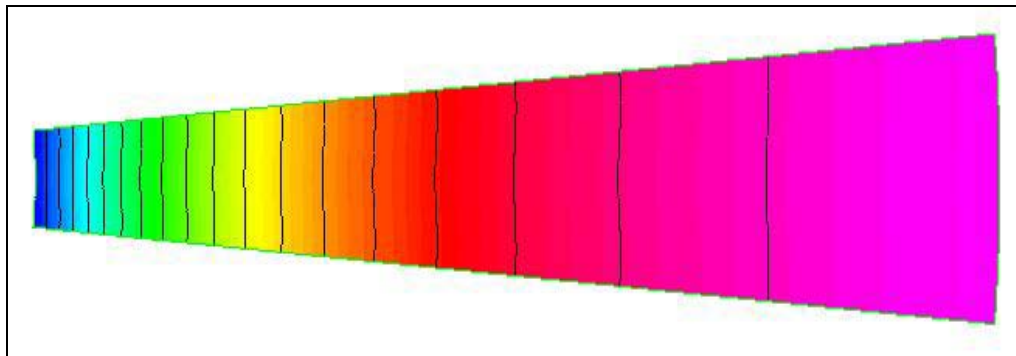


Figure 13.        Static pressure contours.

Comparison of the numerical to the analytical solution in terms of velocity profiles is given in Fig.9. This plot presents the non-dimensional velocity profiles at two

stations namely at x=0.004 m and x=0.007 m along with the exact velocity profile for the same mass flow rate. The agreement between the two solutions is excellent with $\Delta u / u < 0.1\%$.
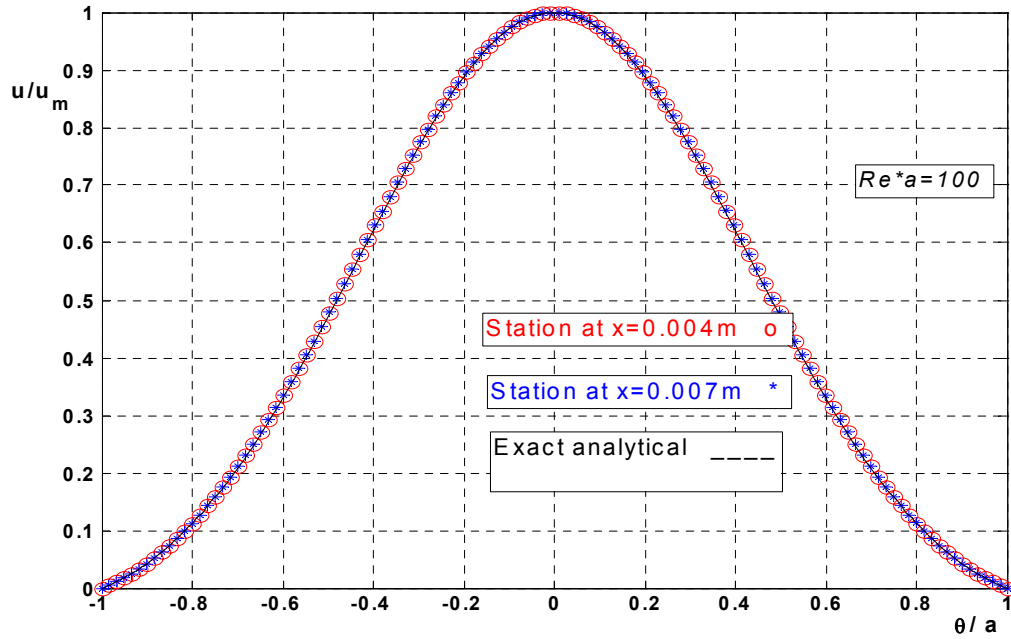


Figure 14. Comparison of the computed velocity profiles with the exact solution

Comparison of the numerical to the analytical solution in terms of static pressure profiles along the centerline is given in Fig.15. The difference $\delta P$ is from a value of 101,325 Pa assumed at the diffuser exit. Again the agreement between the two solutions is satisfactory (~ 1%).
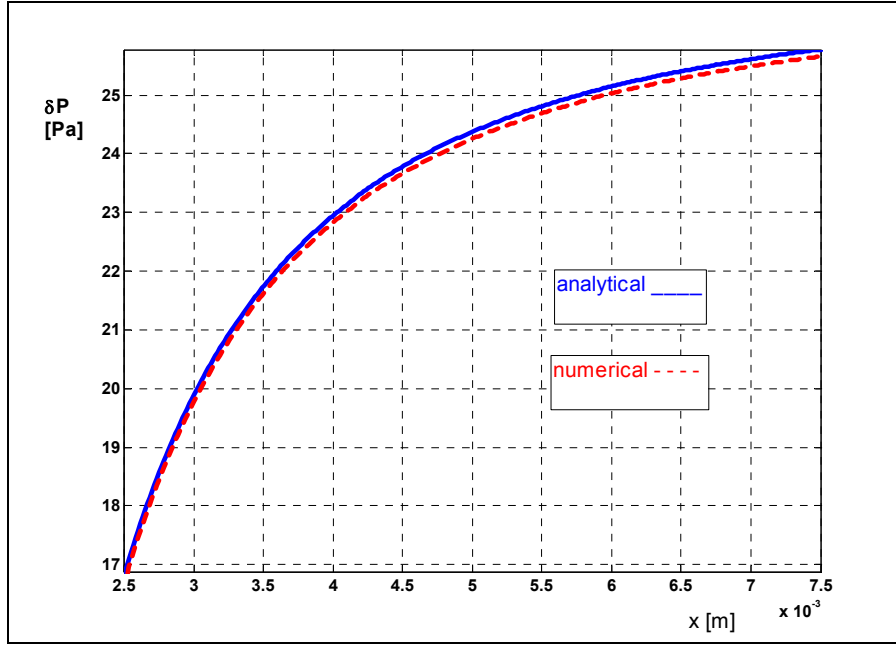
Figure 15.        Comparison of the computed static pressure centerline profiles with the exact

analytical solution

**D.      A NOTE ON THE NON-EXISTENCE OF SIMILARITY SOLUTIONS IN CONICAL DIFFUSERS WITH POINT SOURCE ENTRY FLOWS SINGLE SPACE**

The possibility of existence of similarity solutions in conical diffusers is investigated here. If the flow is assumed purely radial emerging from a point source at the origin and driven through a conical diffuser the analogous 3-D case to the Jeffery-Hamel flows in two dimensions emerges. Equations of continuity and momentum are written in the spherical coordinate system:
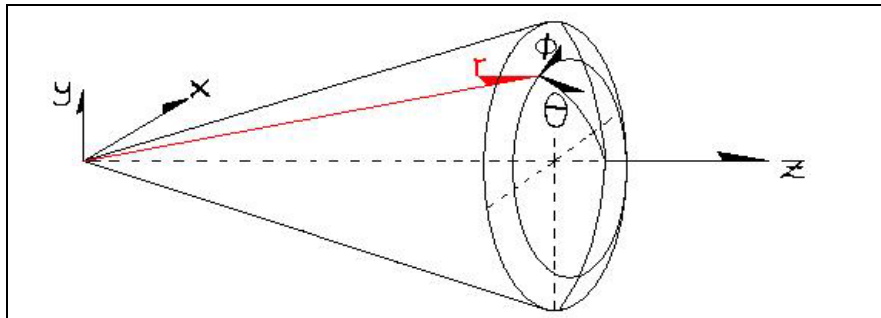


Figure 16.        Conical diffuser coordinate system.

24

$$\frac{1}{r^2}\frac{\partial(r^2 u_r)}{\partial r}+\frac{1}{r\sin\theta}\frac{(u_\theta\sin\theta)}{\partial\theta}+\frac{1}{r\sin\theta}\frac{\partial u_\phi}{\partial\phi}=0 \tag{28}$$

$$\rho\frac{D\vec{V}}{Dt}=-\nabla p+\mu\nabla^2\vec{V} \tag{29}$$

Since the velocity emerging from the point source is assumed to be purely radial, the $u_\theta, u_\phi$ components of the velocity must be zero. Substituting in continuity above and integrating once with respect to r we get:

$$u_r=\frac{vF(\theta,\phi)}{r^2} \tag{30}$$

$$u_\theta=0 \tag{31}$$

$$u_\phi=0 \tag{32}$$

We search for a similarity velocity profile $F(\theta,\phi)$. It will be shown in two ways that such a solution does not exist. First by dimensional reasoning (presented here) and then in a more mathematical form presented in the Appendix B. The velocity at the centerline is

$$u_m=u_r(r,0,\phi)=\frac{vF(0,\phi)}{r^2}$$

A Reynolds number can be defined as,

$$\mathrm{Re}=\frac{u_m ra}{v}=\frac{v[F(0,\phi)/r^2]r}{v}=\frac{F(0,\phi)}{r}a$$

Where $a$ is the diffuser half angle.

This number gives the ratio of inertia to viscous forces inside the diffuser. If $F(\theta,\phi)$ were a similarity profile, then $F(0,\phi)$ at the centerline would be invariant. Since $a$ is constant, Re number is a function of r. Thus Re number is not invariant meaning, the ratio of the inertia to viscous forces decreases downstream. Thus similarity solutions to the Navier-Stokes equations for this type of flows do not exist. On the contrary this is not

25

the case for the 2-D plane diffusers presented in the previously. There, the Reynolds number is defined as,

$$Re = \frac{u_m r a}{\nu} \tag{33}$$

And the centerline velocity as,

$$u_m = \frac{F(\theta)}{r} \tag{34}$$

Substituting in (21) above,

$$Re = \frac{\dfrac{F(\theta)}{r} r a}{\nu} = \frac{F(\theta) a}{\nu} \tag{35}$$

Thus Reynolds number is clearly invariant throughout the flow field since $\alpha$ and $\nu$ are constants. This means similarity solutions are possible in this case.

# IV. NUMERICAL SIMULATION OF INCOMPRESSIBLE LAMINAR STEADY FLOW IN 2-D DIFFUSERS WITH EXIT CHANNELS

## A. OVERVIEW

Direct numerical simulation will be presented to investigate performance and various flow regimes that might exist in 2-D plane laminar diffuser flows at Reynolds numbers range of 105-1048. Channels are situated upstream and downstream of the diffuser. A number of different geometries (AR=1.15 through 5 and $L/W_1$=1-48) are considered. The diffuser inlet flow is assumed incompressible, laminar and fully developed.

## B. DEFINITION OF THE PROBLEM

### 1. Geometric Configuration

The general configuration used in this study and the appropriate geometric parameters that describe it are shown in Fig.17. In this figure $W_1$, $W_2$ are the inlet and outlet heights of the diffuser, L is the length of the diffuser.
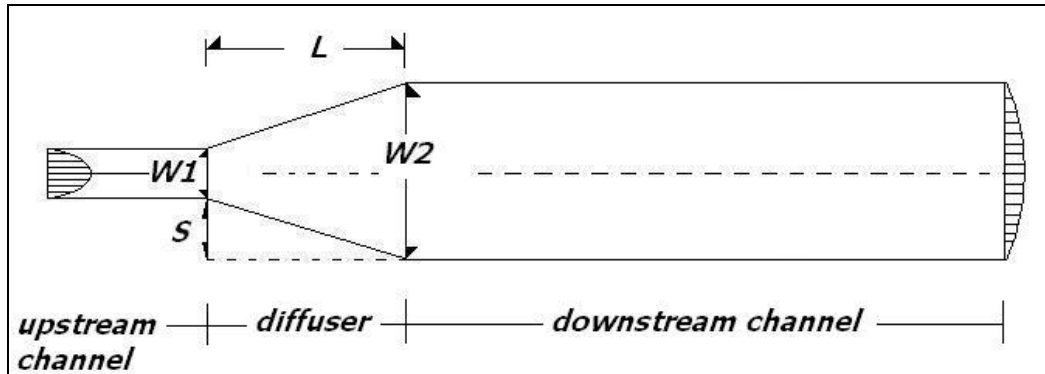


Figure 17. Diffuser-inlet-exit channels general outline.

The area ratio is varied from 1.15 to 5 and the length to inlet height $L/W_1$.is varied from 1 to 48. Inlet and outlet channel lengths are chosen with appropriately large length to accommodate properly the flow inlet and outlet boundary conditions. It is explained later why and how these lengths are chosen.

## 2.    Simulations Matrix

For the geometries mentioned in 1 above, Reynolds number runs of 63, 84, 105,

210, 314, 420, 629, 839 and 1048 will be performed. The Reynolds number is

defined as:

$$Re = \frac{U W_1}{\nu}$$

Where $U$ is the mean inlet channel velocity, $W_1$ is the inlet channel height and $\nu$

is the kinematic viscosity. The specific test geometries in terms of area ratio and non-

dimensional length are shown in Figure18 on a log-log graph.



Figure 18.        Diffuser geometries tested.

The same information in different form is given in Table.1 where the diffuser half

angles in degrees are included. Geometries of half angles more than 45$^o$ and less than 1$^o$

are discarded. At the 45$^o$ angles the grids become skew enough to influence the accuracy

and convergence of the solution and at 1$^o$ and below geometries are of no practical

28

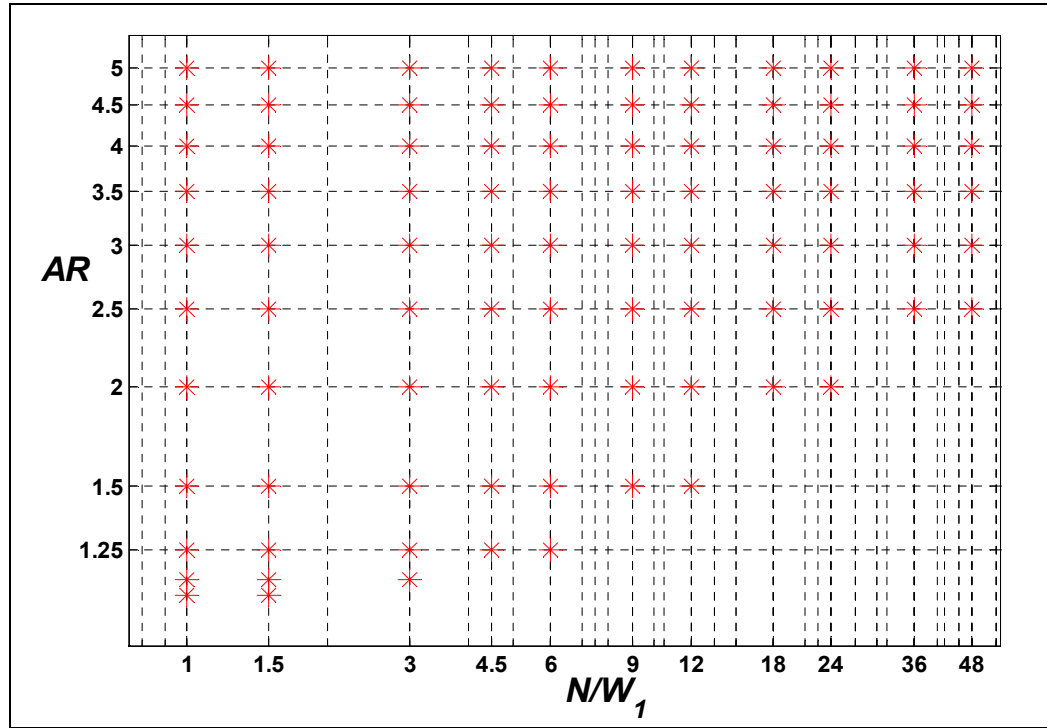interest. For all diffuser geometries the flow is computed for the different Re numbers mentioned before. Every such run will be referred to as a "case" from now on. For instance a diffuser of non-dimensional length 4.5, area ratio 3.5 and Re number 314 is the "case" 4.5_3.56. Table.2 contains Re numbers and max centerline velocities for all cases.

Table 1     Diffuser geometries tested.

| AR→ | 1.1 | 1.15 | 1.25 | 1.5 | 2 | 2.5 | 3 | 3.5 | 4 | 4.5 | 5 |
|---|---|---|---|---|---|---|---|---|---|---|---|
| Set48 | | | | | | | 1.19 | 1.49 | 1.79 | 2.08 | 2.38 |
| Set36 | | | | | | 1.19 | 1.59 | 1.98 | 2.38 | 2.78 | 3.18 |
| Set24 | | | | | 1.19 | 1.79 | 2.38 | 2.98 | 3.57 | 4.17 | 4.76 |
| Set18 | | | | | 1.59 | 2.38 | 3.18 | 3.97 | 4.76 | 5.55 | 6.34 |
| Set12 | | | | 1.19 | 2.38 | 3.57 | 4.76 | 5.95 | 7.12 | 8.3 | 9.46 |
| Set9 | | | | 1.59 | 3.18 | 4.76 | 6.34 | 7.91 | 9.46 | 11 | 12.53 |
| Set6 | | | 1.19 | 2.38 | 4.76 | 7.12 | 9.46 | 11.7 | 14.03 | 16.3 | 18.4 |
| Set4.5 | | | 1.59 | 3.18 | 6.34 | 9.46 | 12.5 | 15.5 | 18.4 | 21.5 | 23.9 |
| Set3 | | 1.43 | 2.38 | 4.76 | 9.46 | 14.03 | 18.4 | 22.62 | 26.5 | 30.2 | 33.7 |
| Set1.5 | 1.91 | 2.86 | 4.76 | 9.46 | 18.43 | 26.56 | 33.69 | 39.8 | 45 | | |
| Set1 | 2.86 | 4.29 | 7.12 | 14.03 | 26.5 | 36.87 | 45 | | | | |

Table 2     Reynolds numbers tested for each diffuser geometry.

| Case# | 1 | 2 | 3 | 4 | 5 | 6 | 7 | 8 | 9 | 10 |
|---|---|---|---|---|---|---|---|---|---|---|
| Re | 21 | 63 | 84 | 105 | 210 | 314 | 420 | 629 | 839 | 1048 |
| $U_{max}$ (m/sec) | 0.5 | 1.5 | 2 | 2.5 | 5 | 7.5 | 10 | 15 | 20 | 25 |

### 3.     Grid Types

Grids are generated for each case in CFD-GEOM and then imported in the solver. The two general arrangements are given schematically in Fig.19, 20:
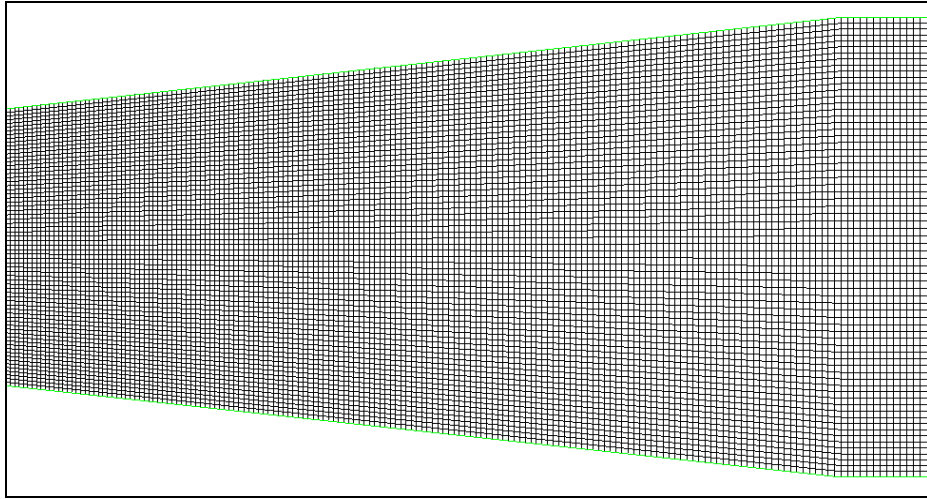
Figure 19.        Grid type1.
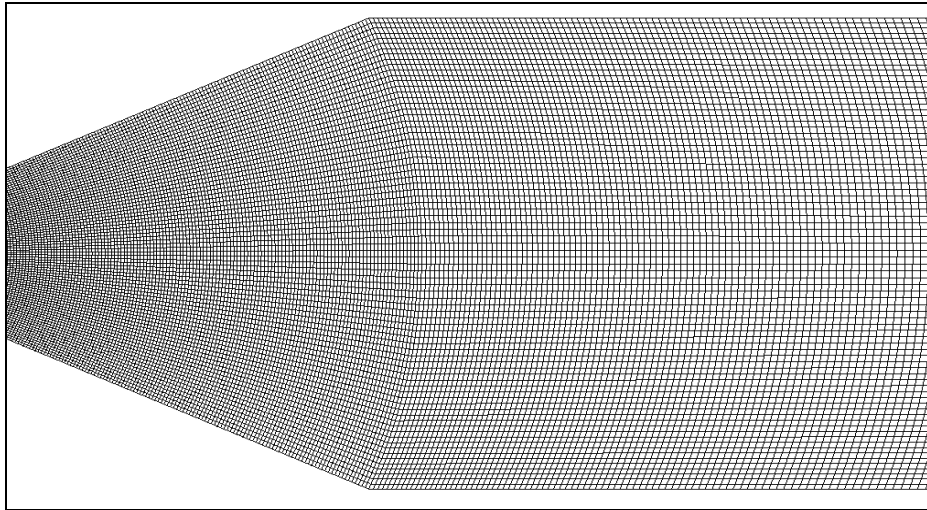

Figure 20.        Grid type2.

Type 2 grids are used whenever the diffuser exit corner angles of type 1 grids become less than $70^o$ i.e. for geometries where half diffuser angle exceeds $20^o$.

**4.        Boundary Conditions**

The types of boundary conditions applied here are:

(1) The no slip, no penetration condition at the walls.

(2) A fully developed parabolic velocity profile at the inlet of the upstream channel calculated in MATLAB and imported in ACE+. The max centerline velocity of this profile is varied according to Table.2.

(3) A uniform static pressure condition at the outlet of the downstream channel.

To determine a good location for the boundaries of the computational domain inlet and outlet so that the boundary conditions would be satisfied sufficiently, the following guidelines were followed. For the upstream boundary, where the parabolic profile would be imposed, the streamlines should have to be parallel. Separate computations (performed in MATLAB using a finite difference method) showed that for potential flow through a sudden expansion with area ratio 5 (the max area ratio used in this study) the streamlines were parallel at a distance $5W_1$ upstream the expansion. Thus an upstream channel length of $8W_1$ was chosen throughout this work. For the downstream exit boundary the streamlines should again be parallel for the uniform pressure to be imposed. Thus channel lengths of $80W_1$-$120W_1$ are used, based on preliminary studies, done by the writer and several other studies such as in ref. [18]. See Appendix.C for the MATLAB coding and results on the potential flow through the sudden expansion.

## C.    NUMERICAL SOLUTION IN ACE+

### 1.    Description of Solver Settings

The "flow" module of ACE+ is used. That means continuity and N-S equations will be solved numerically in two dimensional, steady, incompressible forms. Air at atmospheric conditions will be used as the medium. Inlet channel max velocities will be of the order of 1.5 to 20 m/sec. To keep flow laminar and Re in the desired interval, inlet channel width is chosen to be 1 mm. All other lengths are scaled accordingly in millimeters. Guess values for velocity and pressure should be used to initialize the flow field. Following the manual, the exit static pressure is used as initial value for the pressure field in order to achieve faster convergence. A value for velocity from Table.2 is used throughout depending on the particular run.

Numerical results are digitally stored in '.'. DTF files, named as follows: A diffuser of non-dimensional length 4.5, area ratio 3.5and Re number 320 is the file 4.5_3.56.DTF. The last digit specifies Re number from Table.2. The folder containing all

the runs for the 4.5_3.5 geometry specified above would be named D_4.5_3.5. Thus this folder would contain DTF files such as 4.5_3.54.DTF, 4.5_3.55.DTF, 4.5_3.56.DTF…etc.

## 2. Convergence of the Numerical Solution

As already mentioned above, a number of runs will be performed for the various geometries and Reynolds numbers. For each "case" the residual history of the dependent variables and the "mass flow summary" was recorded. Depending on diffuser geometry and Re number, a general trend was singled out throughout the computations. Specifically, for certain combinations of diffuser geometry and Re number the residual curves obtained had a form shown in the following Figure 21:
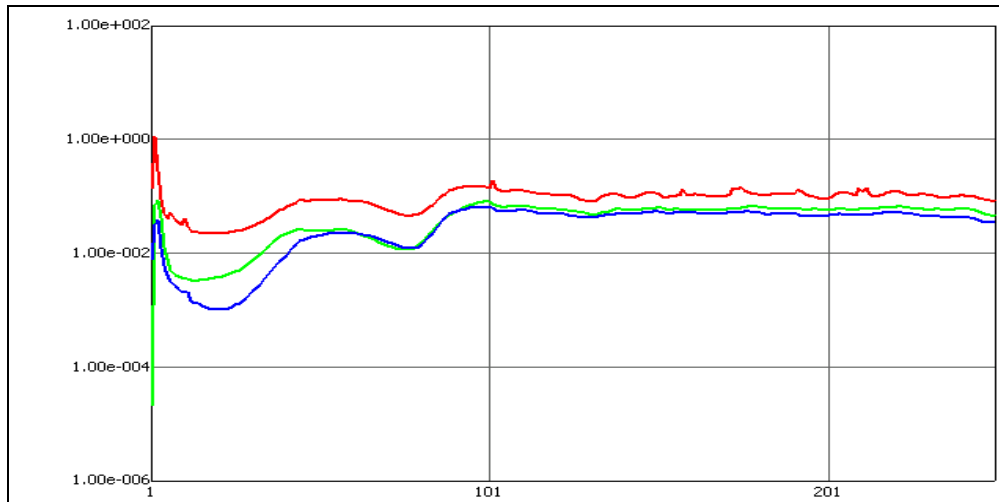


Figure 21.        Typical residual history in non-converging case.

In these cases the computer programm neither converged nor diverged. The "mass flow summary" was very poor meaning continuity was satisfied no better than two to three orders of magnitude and generally more that six orders is sought. Velocity contours for two successive iterations of the same case are shown in Figure.22. It is evident that the flow field changes back and forth without converging to a particular form.
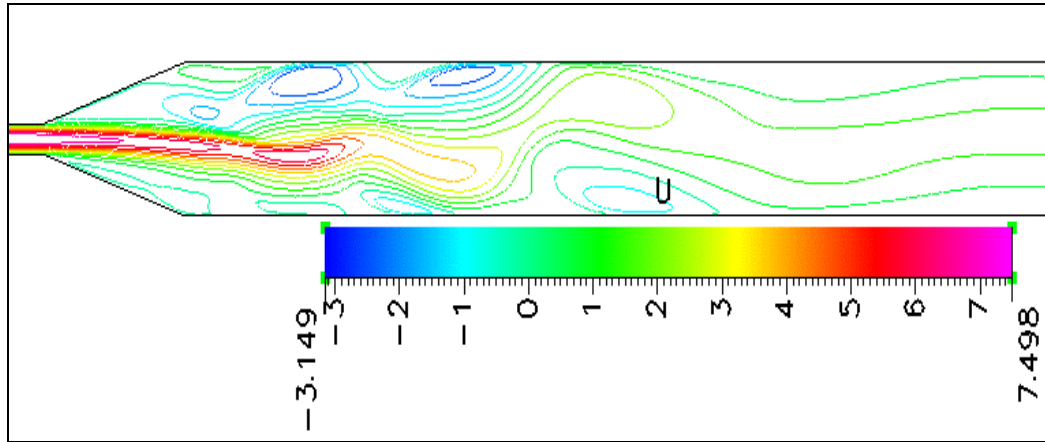
Figure 22.        Non-converging case velocity contours.

For other cases the solution converges in less than 1500 iterations and the residuals have droped at least seven orders of magnitude. Mass flow summaries are very good indicating continuity satisfaction of at least nine to ten orders of magnitude. Figures 23 and 24 show residuals and u velocity contours for such cases respectively:
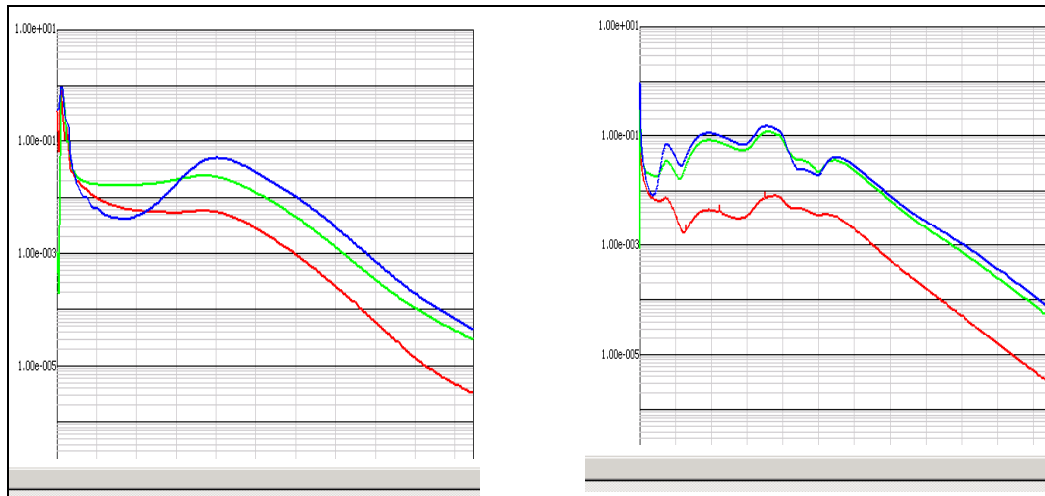


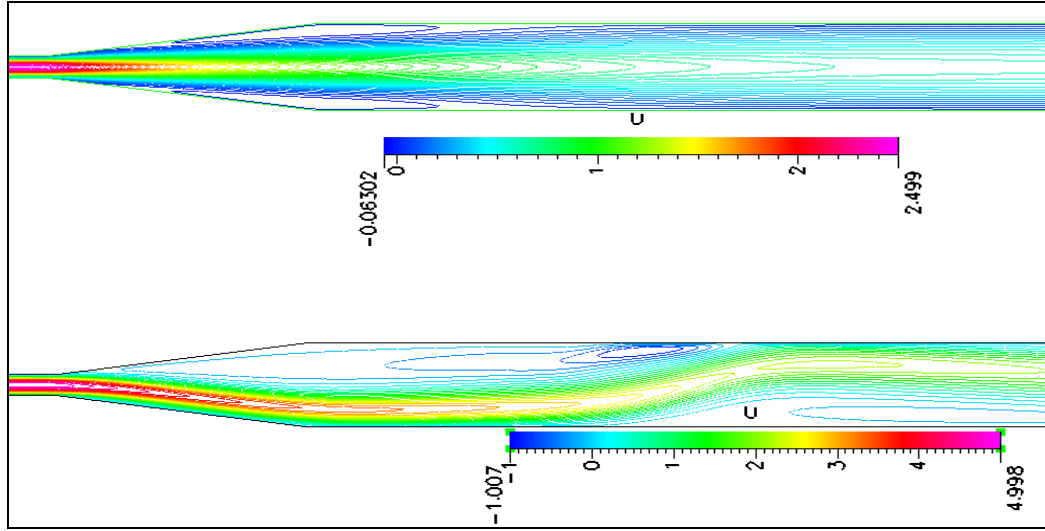Figure 23.        Typical residual history in steady converging cases.

Figure 24.        Typical converging case velocity contours. Top symmetric separated flow.

Bottom asymmetric separated flow.

The distinct trend of the residuals and mass flow summaries is observed in all steady computations. As will be discussed later this trend will be the decisive factor for distinguishing flow regimes.

### 3.        Grid Independence Study

All numerical calculations are performed solving the descretized form of the appropriate differential equations on a finite grid. It is well known that the density of the grid has a significant impact on the accuracy and convergence of the computations. Thus we need to perform a grid independence study until a grid density is found that gives a grid independent solution.

In this study computations on various grid densities were carried out at Re numbers 420 and 630 on diffusers of non-dimensional length $L/W_1= 24$ and area ratios of 3.5, 3 and 2.5, 3 respectively. Two diffuser grids are examined. One more dense and one less dense than the nominal one used for the bulk of the computations. Since the nominal 24set diffuser grid dimensions are (500X80), a denser grid (750x100) and a coarser grid (300x60) are employed for grid independence study. The results are compared to see if the solutions deviate from one another. It is found that good agreement between the three solutions exists. Velocity profiles and centerline static pressure distributions will be

compared for cases where convergence is achieved. For cases where convergence is not achieved the residual histories will be compared.

The results of the grid independence study are shown in Figures 25 and 26. Good agreement is observed between the solutions (relative difference less than 1%)
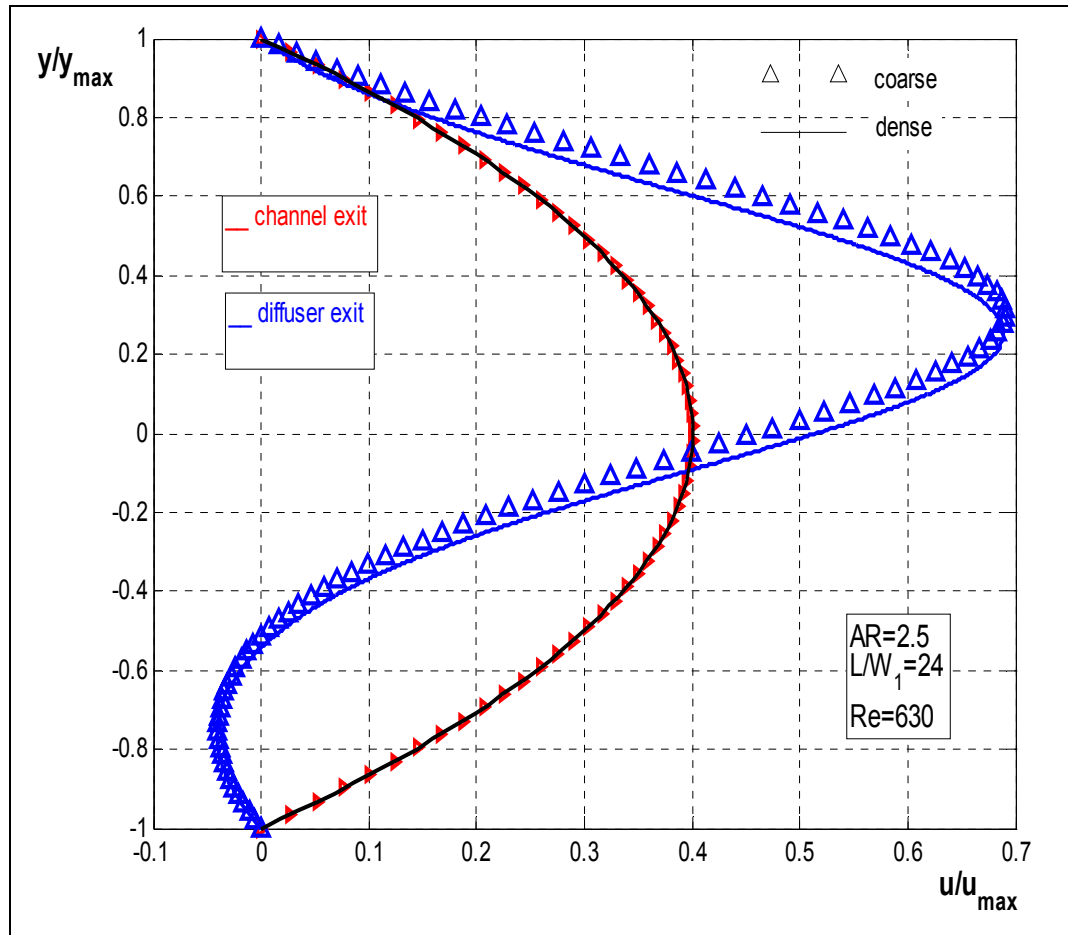
Figure 25.      Velocity profiles comparisons with different grid density.
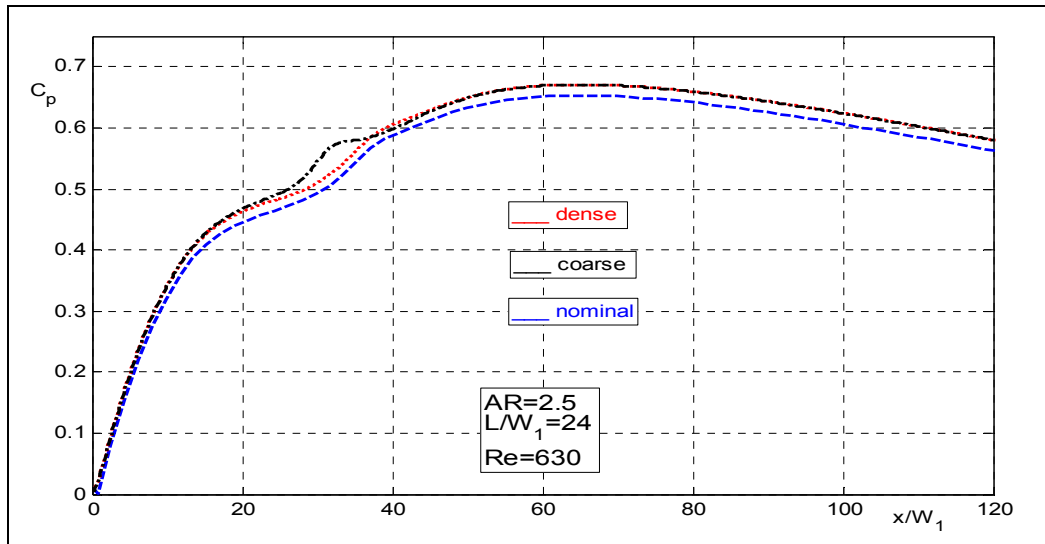
Figure 26.        Comparison of centerline static pressure coefficient in terms of non-
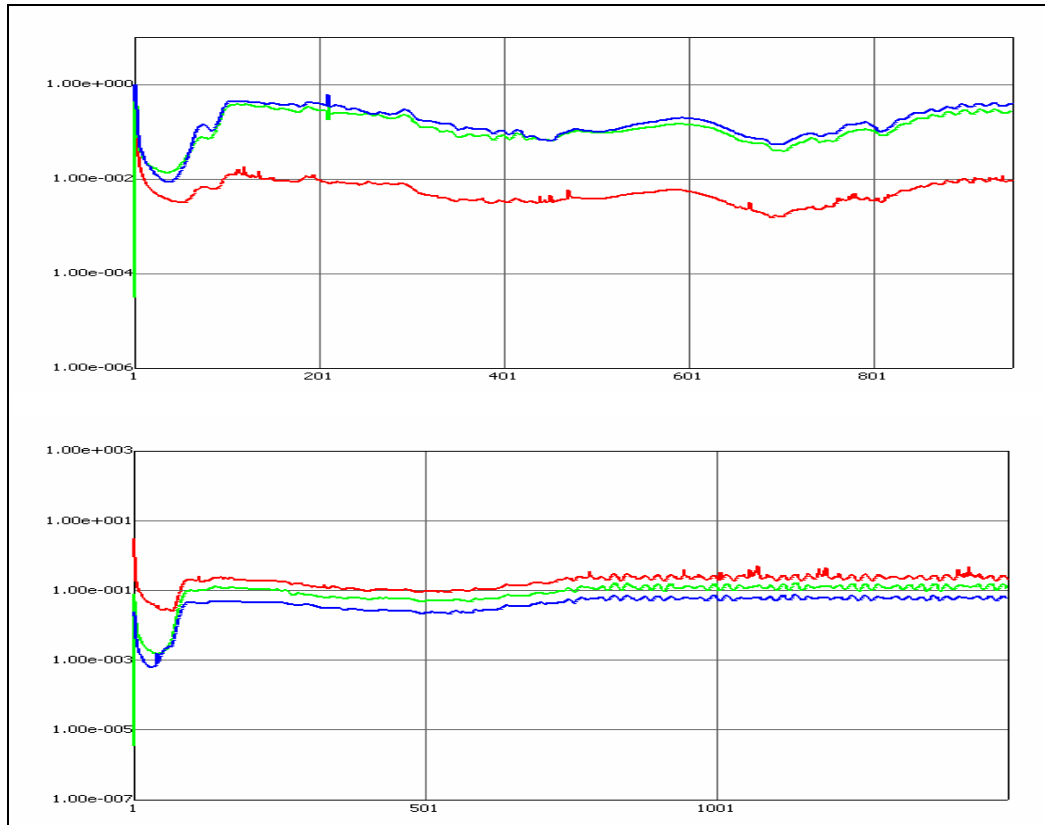dimensional length for grids of different spatial resolution.



Figure 27.        Residuals vs. iteration number comparison for the coarse and dense grid non-
converging cases at Re=629 respectively.

## D.    COMPUTATIONAL RESULTS AND DISCUSION

Residual histories of the primary dependent variables (two velocity components and pressure) and the "mass flow summary" are the criteria distinguishing flow regimes. Cases where residuals are of the form of Figures 21 and 27 and mass flow summary is poor are characterized "non 2-D", meaning that the flow is no longer two-dimensional or time independent. Although the boundary conditions are time independent, the flow is unsteady and/or 3-D and as a result the steady two-dimensional equations are no longer suitable to describe the phenomena inside and downstream the diffuser. Cases where the residuals are of the form of Figure 23 are characterized steady. The flow is two-dimensional steady, separated from one or both diffuser walls except for very low angle geometries were it is not separated at all.

### 1.    Flow Regime Maps

Figure 28 depicts a simple sketch of the different flow regimes identified in this study for a single Re number.
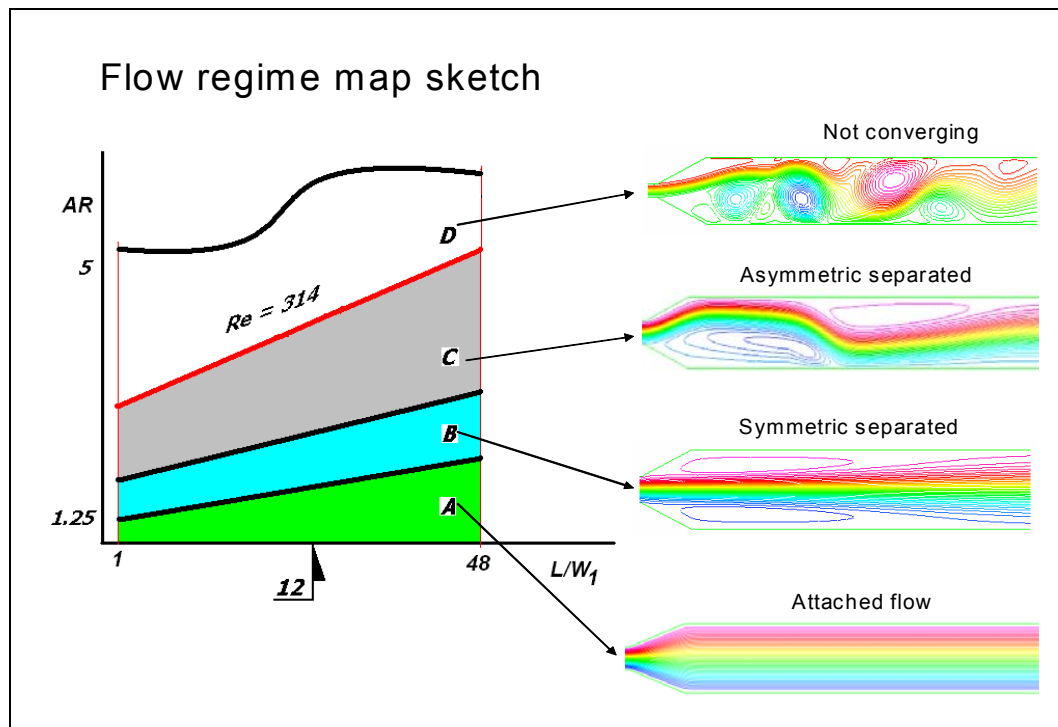


Figure 28.        Flow regime map sketch for Reynolds number of 314.

As the divergence angle is increased there are four regions of different flow configurations observed. Starting at the arrow for example at $L/W_1=12$ the first solid line marks the attached steady flow regime A. Increasing the angle of divergence we enter region B were the flow in the diffuser is symmetrically separated. Increasing the diffusion angle further, region C is reached, where the flow is separated but asymmetric relative to the diffuser centerline. Above the line between C and D is the region where the numerical solution of the 2-D equations neither converges nor diverges. The lines between A B and C regions are qualitatively drawn that far apart because attached and symmetric separated flows occur for very low divergence angles (2-4 degrees) so in a quantitative graph they would be very close. Region C is the one that takes up the largest space in the map below the Re=314 line.

The line between regimes C and D is the one computed quantitatively and is given in Figure 29 for six different Reynolds numbers. Appendix D explains the process by which Fig.29 is extracted from the numerical data. Above the lines in Fig.29, where there is no convergent 2-D steady solution, the flow is believed to be three-dimensional and unsteady. Figure 22 depicts velocity contours of such flow where it can be seen that the contours form an unphysical configuration that more likely depicts a snapshot of three-dimensional unsteady flow vertical center plane cut.
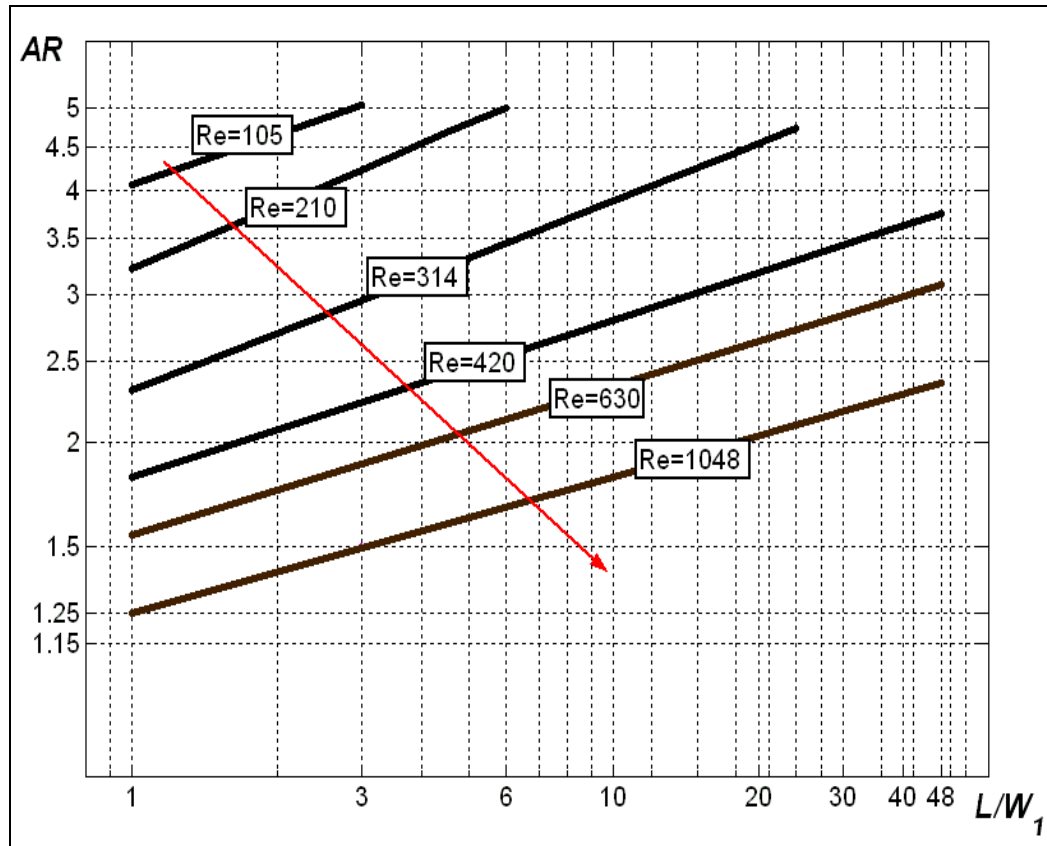
Figure 29.        AR-L/W$_1$ flow regimes map.

A different form of Fig.29 is given in Fig.30. In this figure the power laws derived for the lines in Fig.29 and presented in Appendix D are used to correlate the data in a plot of AR vs. Re number with parameter L/W$_1$. Notice that the lines out of the box in Fig.30 are extrapolations to the data and should be used with caution.

Contrary to the high Re number regime map which only shows geometry dependence of the flow regimes, at low Re numbers with fully developed laminar flows entering the diffuser, the flow regimes depend strongly on diffuser geometry and Reynolds number. With increasing angle the flow goes from attached to symmetric separated to asymmetric separated and finally to a configuration that is not 2-D but is believed to be three dimensional and/or unsteady. There is no region of transitory stall present between the attached and 2-D asymmetric separated regimes.
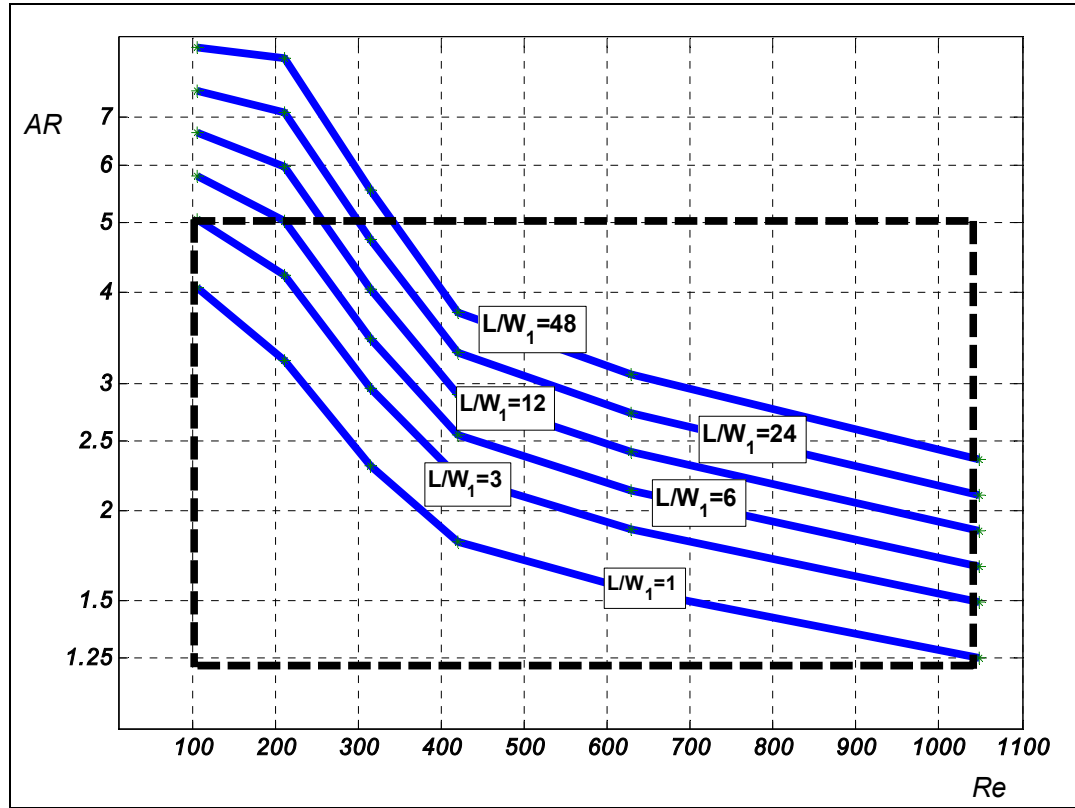
Figure 30.　　AR-Re flow regimes map.

## 2.　　Flow Visualization Graphs

To gain a better visual understanding on the different flow configurations described on the regime map the following graphs may be used. Figures 31, 32, 33 and 34 depict velocity, streamline and static pressure contours respectively. Point tracing emphasizes recirculation regions of the flow. For low diffusion angles the flow is attached, then goes to separated symmetric, then to separated asymmetric and finally it takes the configuration of Fig.33 where the 2-D flow brakes down to what is believed to be the onset of three dimensional and/or unsteady flow. The pressure field is for the symmetric cases is fairly uniform but becomes less uniform for the asymmetric separated case.
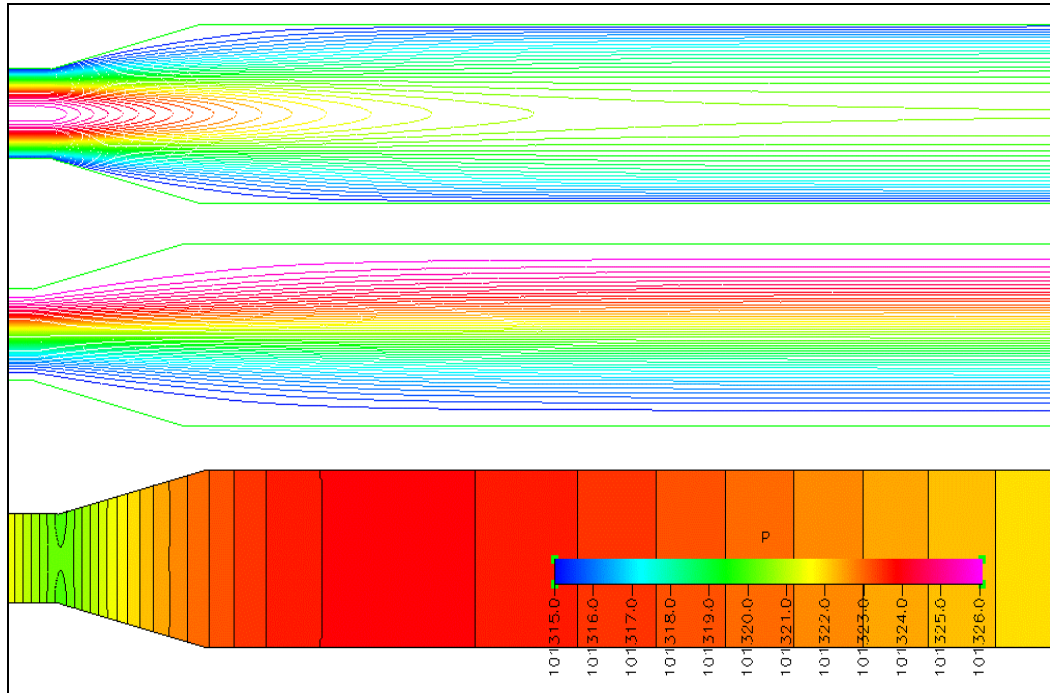
Figure 31.    Velocity, streamlines and static pressure contours for attached flow.
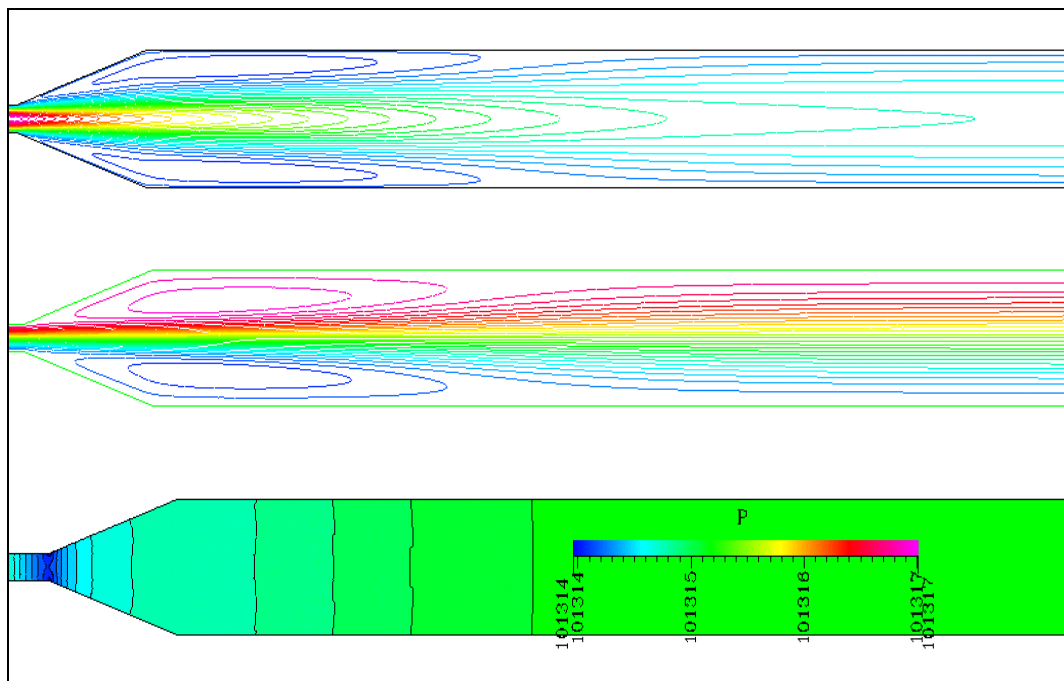


Figure 32.    Velocity, streamlines and static pressure contours for symmetric separated
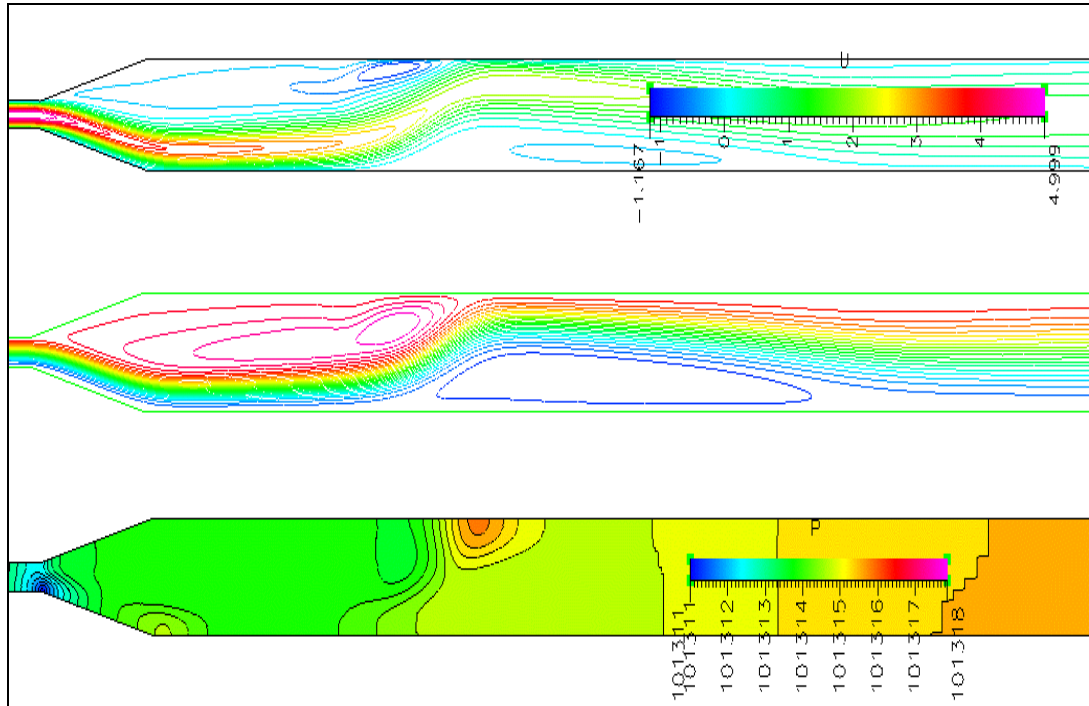flow.

41

Figure 33.        Velocity, streamline and static pressure contours for asymmetric separated
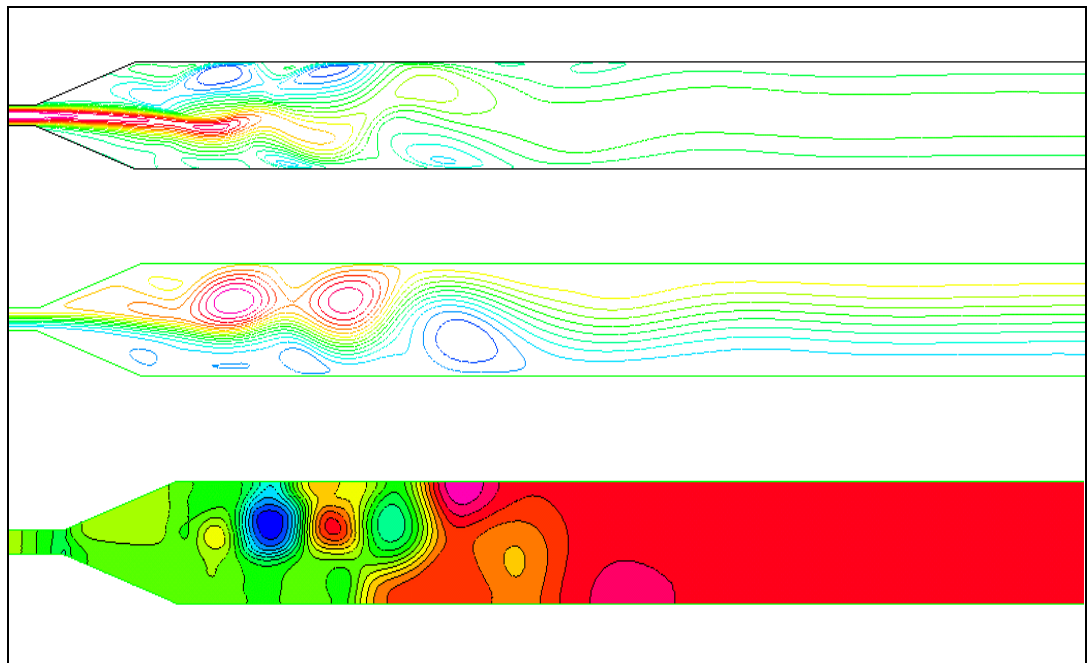flow.



Figure 34.        Velocity, streamline and static pressure contours for a non-converging case.

### 3. Pressure Recovery Maps

A pressure coefficient $C_p$ defined in equation (22) is used to evaluate pressure recovery along the diffuser-exit channel centerline in the flow direction:

$$C_p(x) = \frac{p(x) - p_1}{1/2 \rho U_1^2} \tag{36}$$

The static pressures in all steady 2-D cases (both symmetric and asymmetric flows) were found to be uniform or almost uniform in the y direction. Thus centerline pressure distribution is taken to calculate the value of pressure recovery. A typical $C_p$ vs. $x/W_1$ graph is shown in figure.31. In most of the cases tested the flow is separated from the diffuser walls and reattaches in the downstream channel. These reattachment lengths are twice three times or even longer than the diffuser length. Thus the $C_p$ chosen represents performance of the diffuser and downstream channel together.
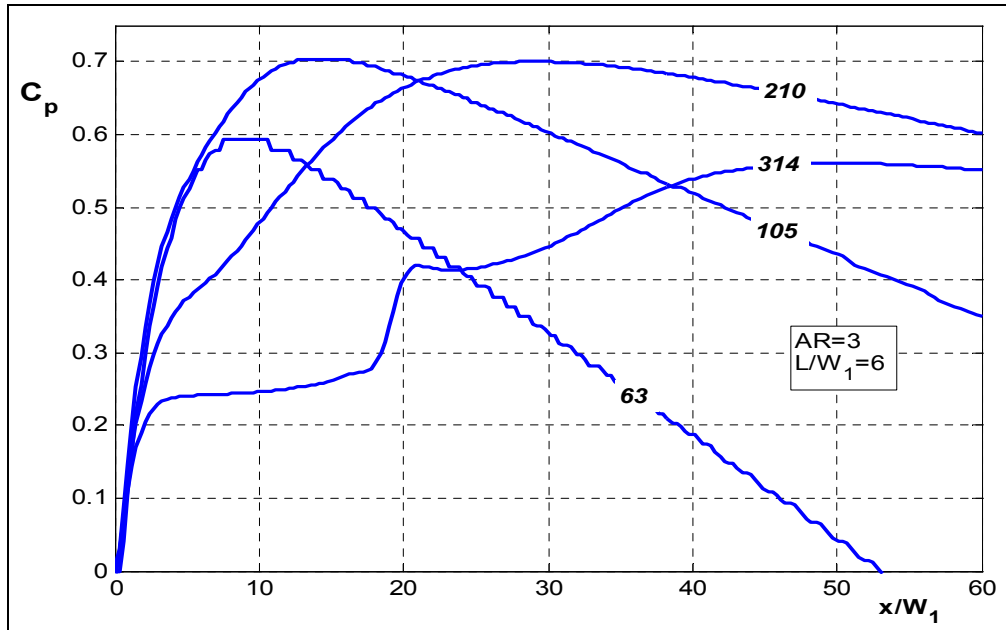


Figure 35.  Typical pressure recovery for different Re numbers along the diffuser-exit channel centerline.

43

Several features in these charts should be pointed out (also discussed in [18]). First the point of maximum $C_p$ does not occur at the diffuser exit but in the down stream channel near the reattachment point. Maximum $C_p$ always shifts to the left i.e. further downstream with increasing Re number since the reattachment point does so also. The $C_p$ maximum does not always increase as the Re number increases while keeping the same geometry but reaches a max value at intermediate Re numbers. This implies the existence of an optimum performance. The wavy pattern of the curves and the consequent overall drop of recovery is the result of the asymmetrical flows. As noted earlier such flow conditions are observed approaching the regime curves from below.

Diffuser-exit channel operating optimums can be extracted from the pressure recovery curves. Such performance maps are constructed if the maximum recovery $C_{p,m}$ is plotted against area ratio and non-dimensional length with Re numbers as parameter and after that the AR-L/W1 cross-plots are taken. Maps at Re=105, 210, 315, 420 and 629 were created. For Re=105, 629 the maps are presented here. The rest three with their respective Cp-AR, Cp-L/W$_1$ graphs can be found in Appendix E. For Re numbers above 629 not enough numerical data exist because of the limitations imposed by the respective flow regime curves.

In Figure 38 and 41 the dotted lines represent the respective flow regime curves on the performance maps. The optimum diffuser performance exists always below these lines. Thus in the case of low Re numbers the max diffuser performance does not exist in the unsteady regime which is above the curves but below the regime lines in the two dimensional asymmetric flow regime. The opposite happens in high Re flows where a diffuser in the transitory stall regime exhibits the best pressure recovery.

The flow regime lines in Figure 29 are approximately lines of constant diffusion angle. In this context maximum pressure recovery in low Reynolds number diffusers takes place for increasing diffusion angle as Re decreases. This is in contrast to high Re diffusers where the maximum recovery comes for a single diffusion half angle of 6-7 degrees.

44
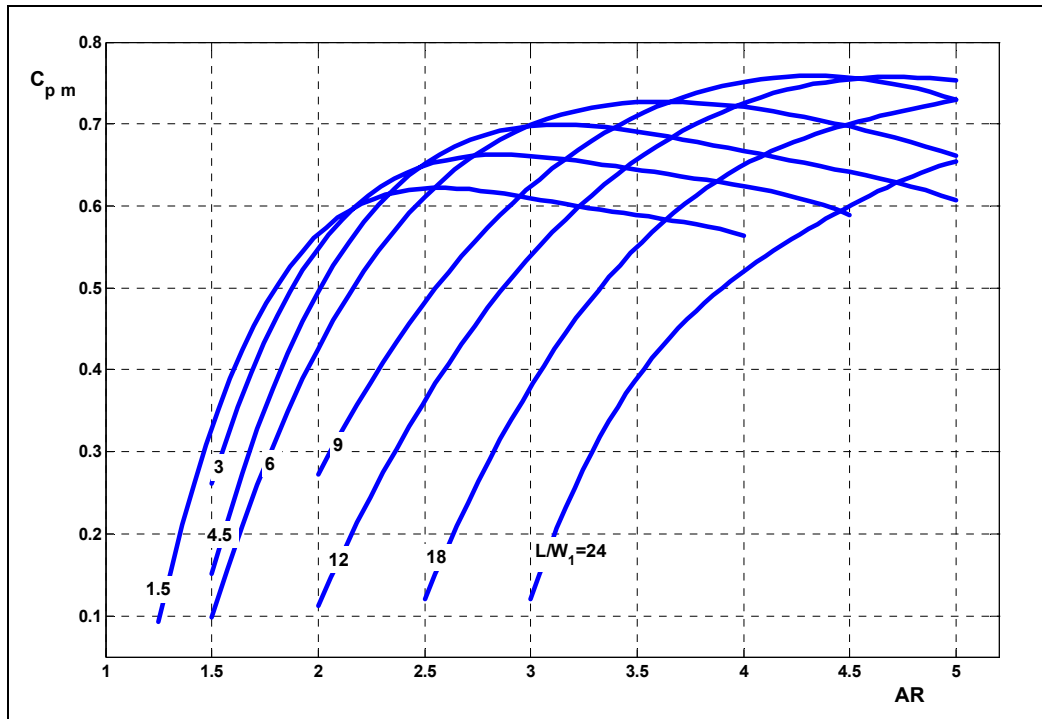
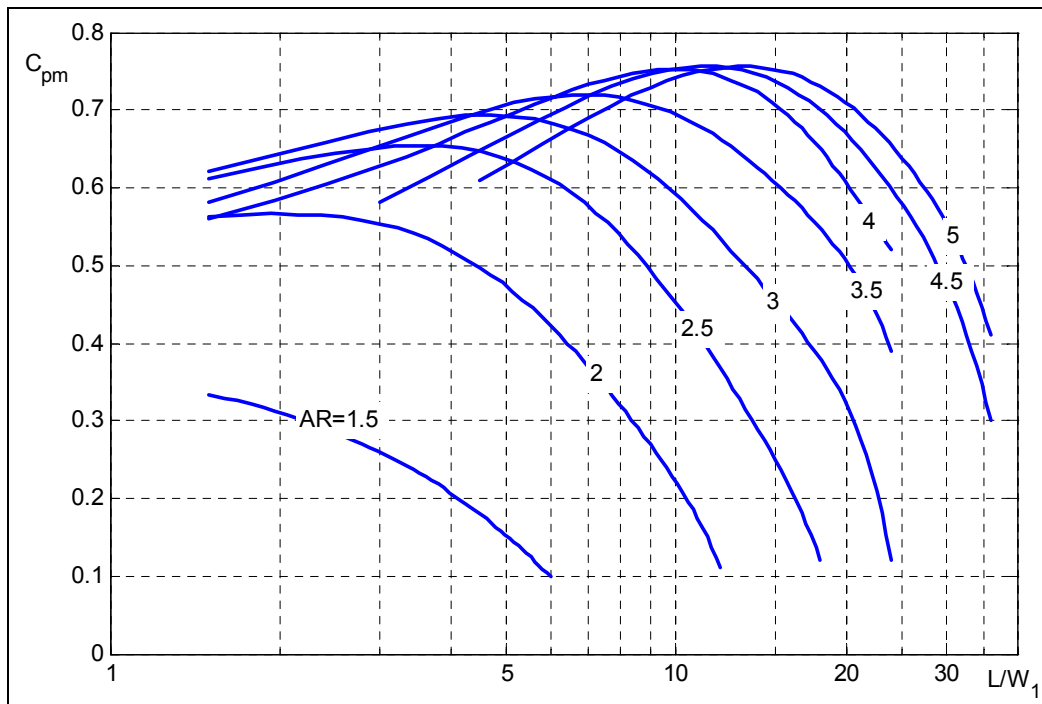Figure 36.        Variation of maximum $C_p$ with AR for Re=105.



Figure 37.        Variation of maximum $C_p$ with $L/W_1$ for Re=105

45
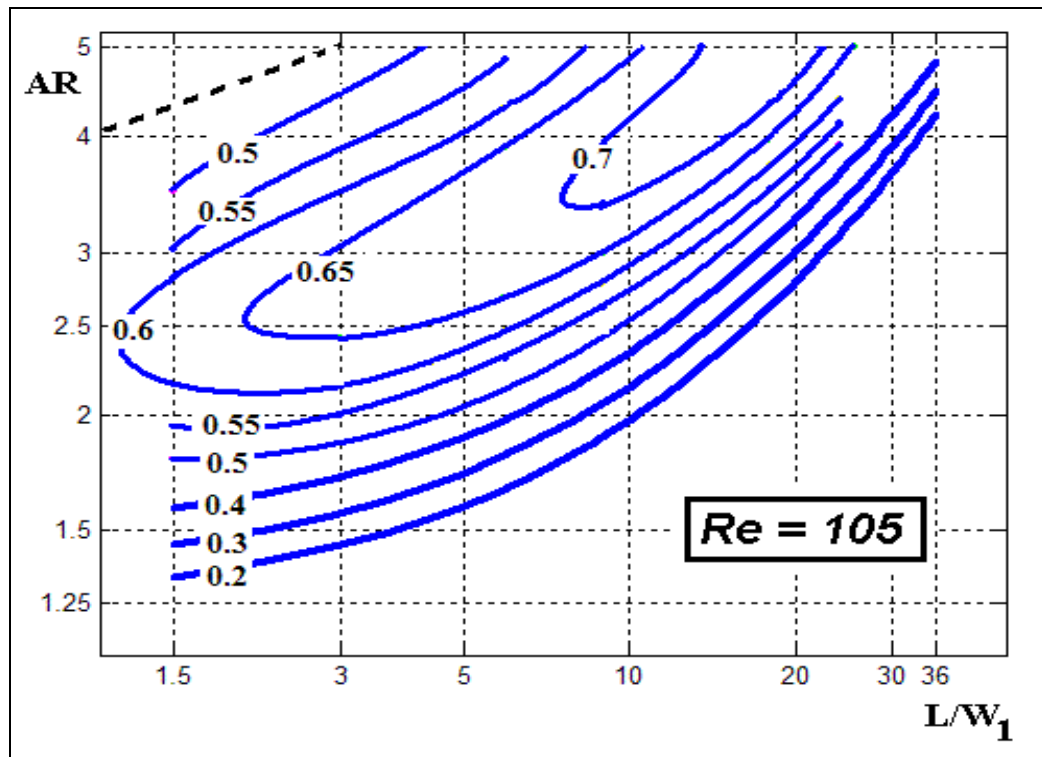
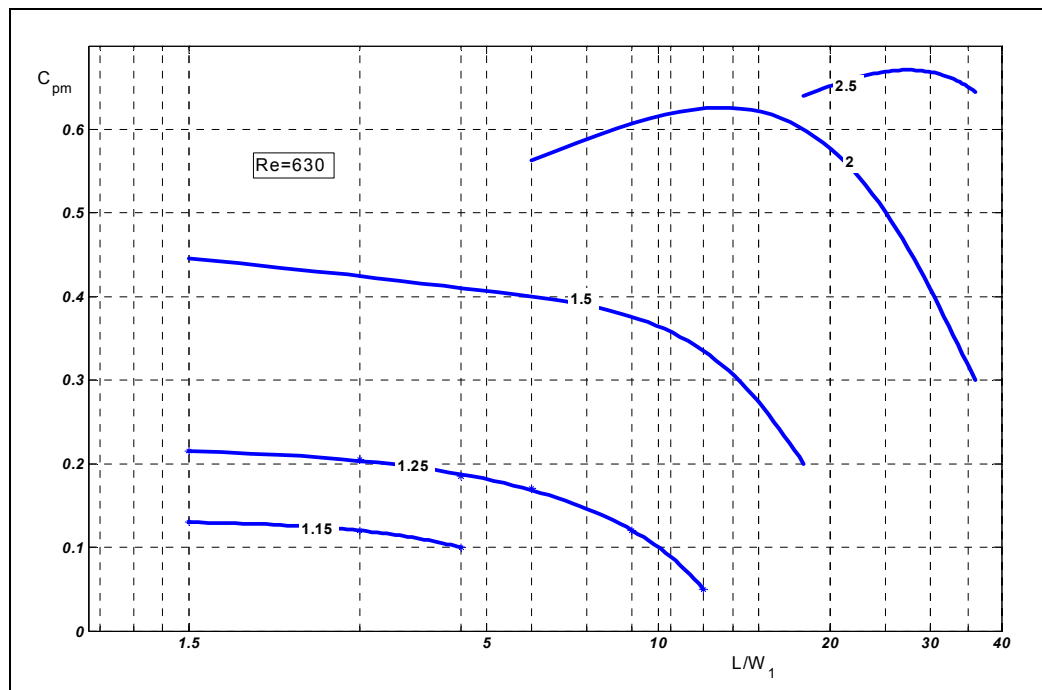Figure 38.　　AR-L/W$_1$ performance map for Re=105.



Figure 39.　　Variation of maximum C$_p$ with L/W$_1$ for Re=629.

46
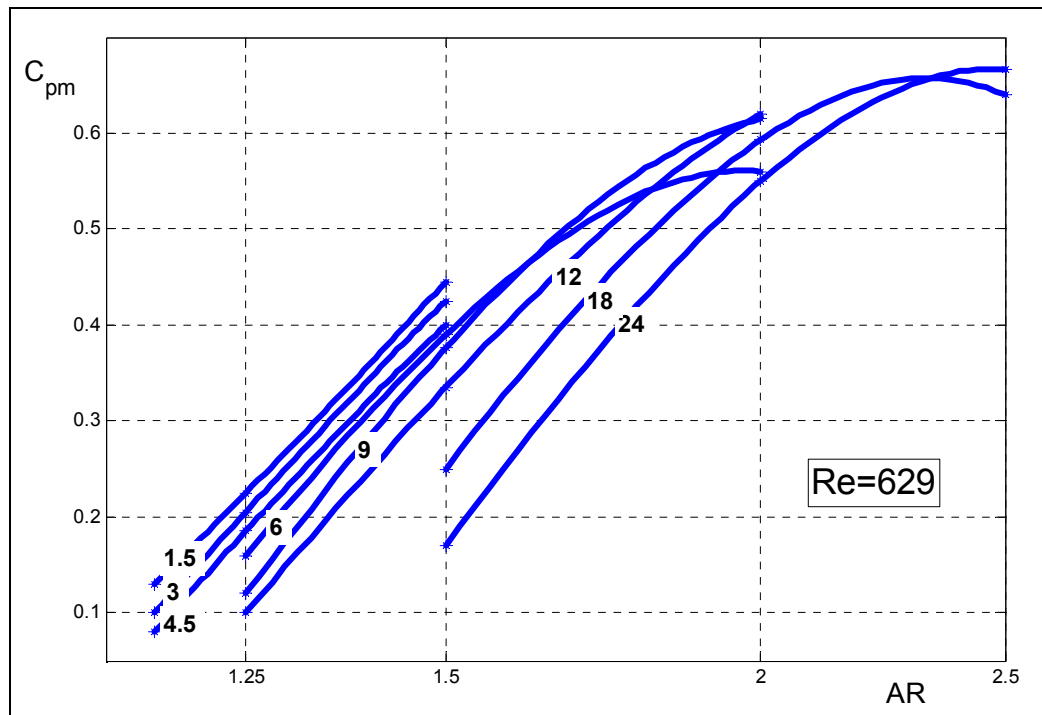
Figure 40.        Variation of maximum $C_p$ with AR for Re=630
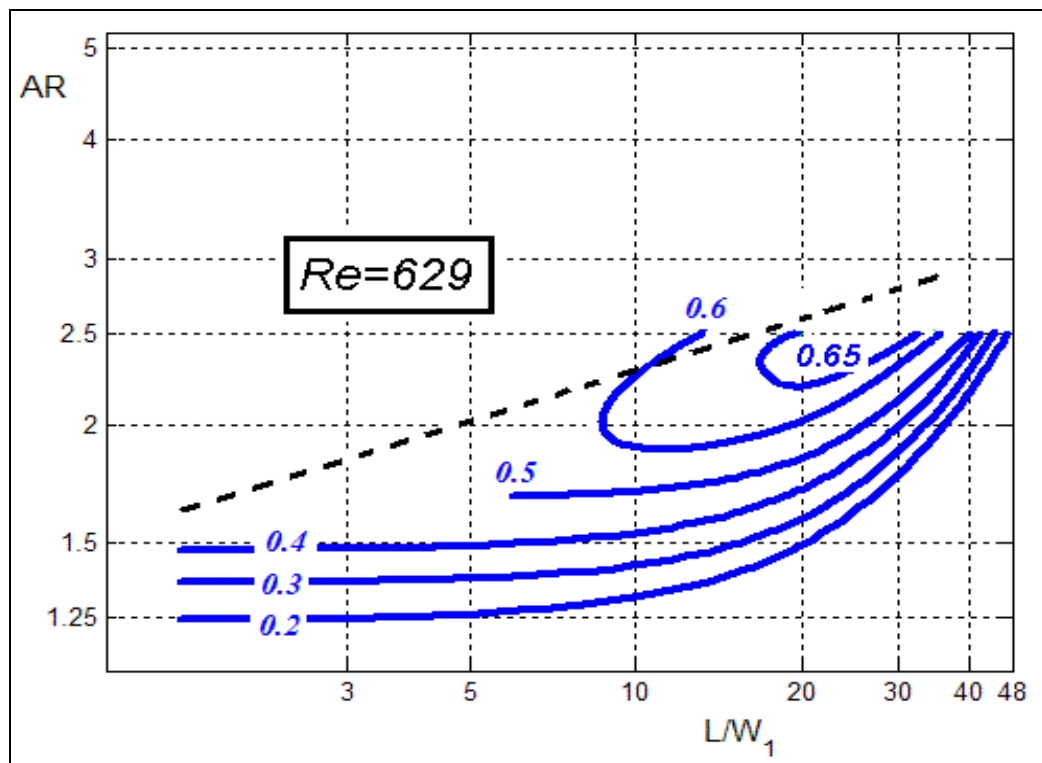


Figure 41.        AR-L/W$_1$ performance map for Re=629.

As Reynolds number increases the optimum region shifts to lower diffusion angles and higher diffuser lengths. As diffuser lengths become smaller recovery should go to a value close to that of an abrupt expansion with the same area ratio. In Figures 37 and 39 the pressure recovery on the left approaches a single value for each area ratio. A simple pseudo-inviscid analysis presented in Appendix C suggests that the maximum pressure recovery achieved with an abrupt expansion is 0.5 when the area ratio is 2. Thus Figures 37 and 39 suggest that it is advantageous to use diffusing passages instead of expansions in order to get higher pressure recovery when the Reynolds number is low.

# V. TIME RESOLVED SIMULATION OF 2-D FLOWS IN DIFFUSERS WITH EXIT CHANNELS

## A. OVERVIEW AND PURPOSE

A time marching time accurate numerical solution of the unsteady 2-D Navier-Stokes equations was attempted here. The flow was impulsively started with a pressure force and after sufficient time approaches a condition that depends on diffuser geometry and Re number. It is attempted to see if the flow approaches the same 2-D condition as when solving the steady equations, for AR-L/$W_1$-RE combinations situated upon and below the two-dimensional flow regime curves computed in the previous chapter. The same time marching procedure is applied to AR-L/$W_1$-RE combinations that lay above the regime lines in an attempt to see what happens to the flow field after a large period of time.

## B. DEFINITION OF THE PROBLEM

### 1. Geometry Configuration, Simulations Matrix and Grid Types

The same basic Fig.15 geometry is considered again for the time resolved solutions. Inlet channel length is modified for reasons explained later. The grid types are the same as the ones used in the steady computations. Different runs will be performed according for the cases described in Table.3. A letter (t) denotes a transient case. The rest is being kept the same as the steady case notation.

Table 3 Time resolved cases simulations.

| | | | | | |
|---|---|---|---|---|---|
| Re=314 | 3_36t | 4.5_3.56t | 6_3.56t | 9_46t | Above b-b |
| Re=314 | 3_2.56t | 4.5_36t | 6_36t | 9_36t | Below b-b |
| Re=210 | 4.5_55t | 1.5_45t | | | Above a-a |
| Re=210 | 4.5_4.55t | 1.5_3.55t | | | Below a-a |

On the flow regime maps the test geometries show as in Fig.41. In this figure the triangles depict cases given in Table.3 above and below the flow regime lines for Reynolds numbers 210, 314.
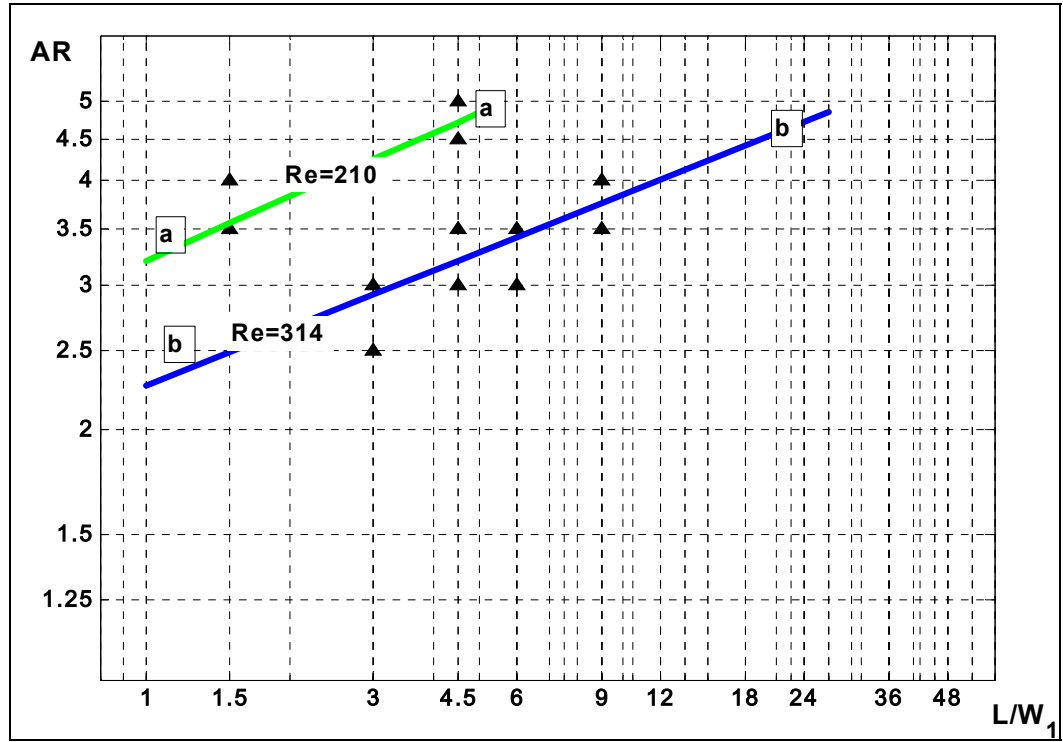
Figure 42.        Unsteady cases on the flow regime map.

### 2.        Boundary and Initial Conditions

For the time resolved simulations a constant total pressure is used at the inlet boundary of the upstream channel. At the downstream channel exit a constant static pressure boundary is imposed. An initial condition of static pressure equal to the exit static pressure and zero velocity throughout is used. The inlet channel length needs to be modified to allow fully developed parabolic flow at the diffuser entrance. An experimentally determined correlation of the following type (see Ref.3) is applied to determine the appropriate upstream channel length:

$$\frac{x}{h} = \frac{0.63}{0.035\,\mathrm{Re}+1} + 0.044\,\mathrm{Re}$$

Thus for Reynolds number 210, 314 minimum lengths of $x/h \approx 10$ and $x/h \approx 14$ are used respectively.

## C.    NUMERICAL SOLUTION IN ACE+

### 1.    Description of ACE Settings for the Transient Computations

The flow module is again used for the transient simulations. Specifying the time step and total number of steps in the appropriate fields the unsteady two-dimensional incompressible Navier-Stokes equations are solved. For all calculations a time step of 0.0015 sec is used. Maximum number of time steps is computed by the max time the flow needs to approach the steady condition. An estimate of max time needed by the flow to approach the steady flow can be taken by an existing exact Navier-Stokes solution for the impulsively starting flows in channels due to pressure gradients. This exact solution gives the following non-dimensional time parameter:

$$\tau = \frac{t\nu}{h^2}$$

For channel flows it is found that the velocity approaches the parabolic shape at:

$$\tau \simeq 0.47$$

Thus for our case, an estimate for the max time the flow needs to approach a final steady condition might be:

$$t = \frac{0.47\,h^2}{\nu}$$

Calculations herein use the viscosity of air 1.589e-5 m2/sec and the height of the exit channel. A 15-20% increase to the above calculated time determines the actual value that is finally used. The overall geometry dimensions are in millimeters. This ensures that the pressure gradient is felt instantly throughout the flow field because the time step used is at least three times more than the time sound waves need to propagate downstream. Under relaxation values of 0.06-0.08 are used for all dependent variables.

### 2.    Convergence of the Transient Solutions

Convergence history of the dependent variables in each time step can be viewed in ACE+. For cases below the lines a-a or b-b on Figure 42, residuals steady out after sufficient amount of time. For cases above the lines this is not true. Residuals continue to converge to the specified criterion in each time step and the flow field solution seems to alternate between several configurations (in each time step). This is believed to be the

51

onset of three-dimensional and/or unsteady flow. The following residual curves are obtained for large periods of time depending on whether the geometry is above or below the flow regime curve of Figure 42.
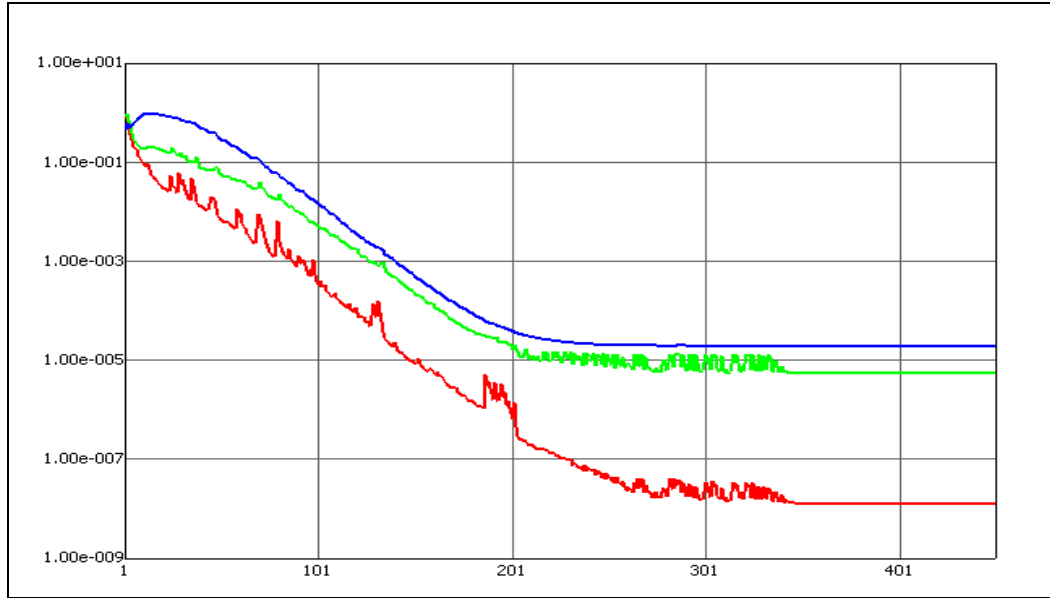


Figure 43.        Typical time step residual history at large times for cases below a-a or b-b.
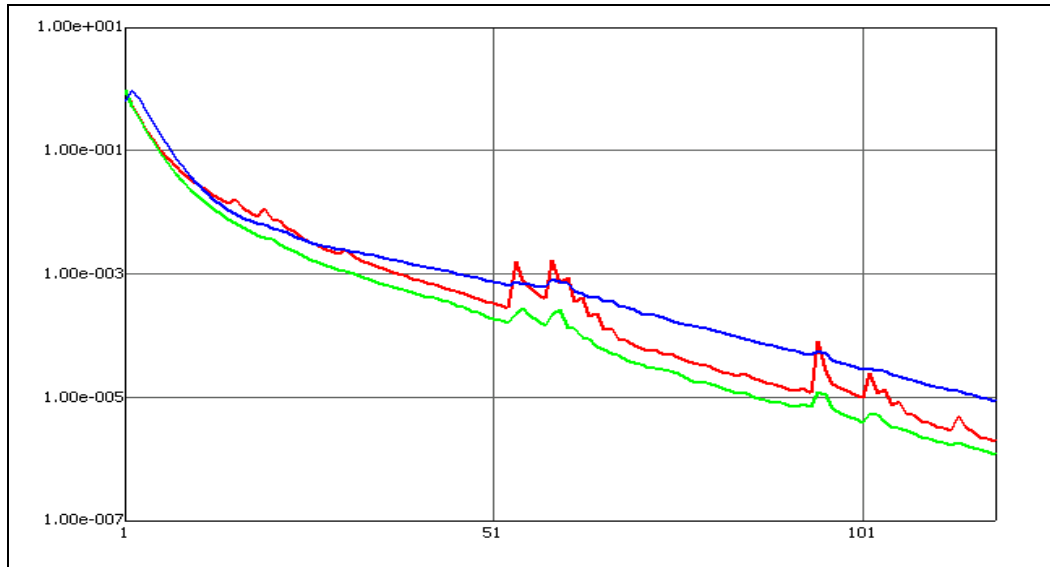


Figure 44.        Typical time step residual history at large times for cases above a-a or b-b.

## D.    COMPUTATIONAL RESULTS AND FLOW VISUALIZATION.

Transient computations results will be presented in terms of evolution in time of velocity profiles and centerline static pressure distributions. These results will be compared with analogous ones computed in the previous chapter for the same geometries and Re numbers only for the steady flow cases. Velocity and streamline contours will be presented for all cases (both above and below the lines (a-a) and (b-b).

### 1.    Instantaneous Velocity and Centerline Pressure Profiles

Velocity distributions in the upstream and far downstream in he exit channel approach the parabolic profiles when the steady flow is reached. The following Figure 44 depicts a typical evolution of velocity profile at the exit of the downstream channel.
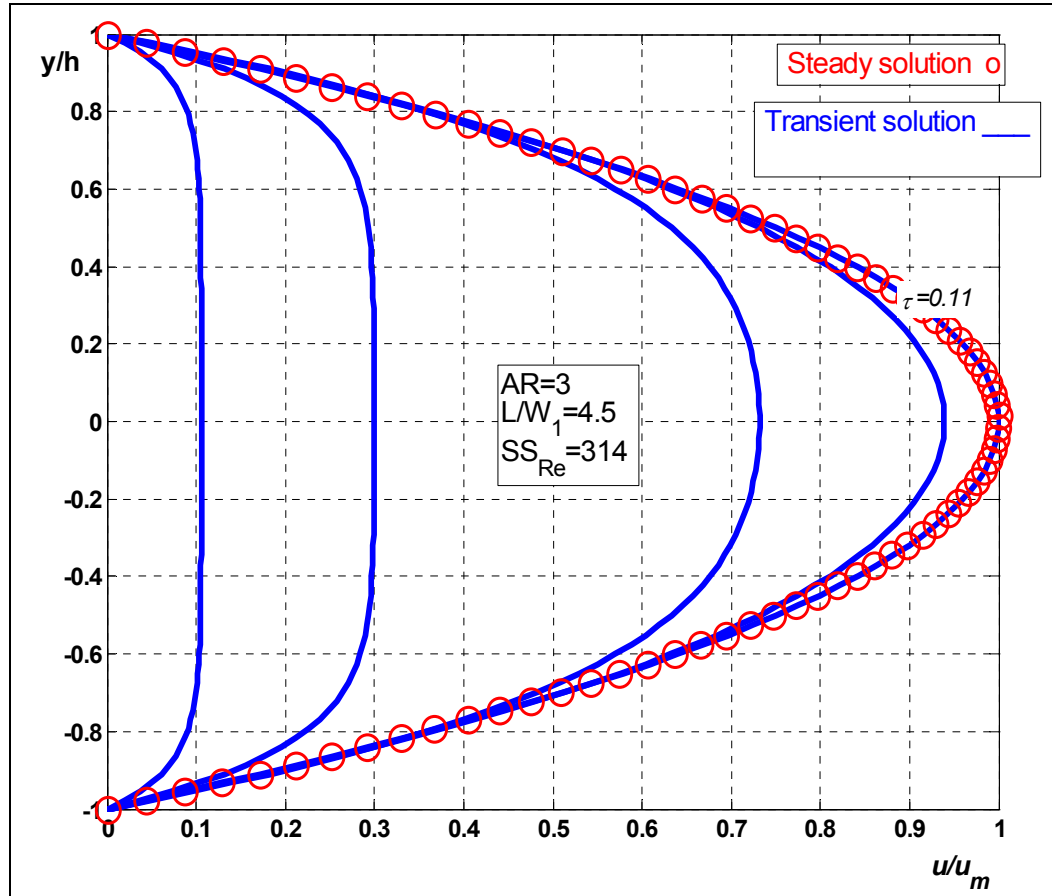


Figure 45.        Instantaneous and final steady velocity profiles.

The non-dimensional time constant for the flow to approach the parabolic profile is found to be 0.11 for downstream channel height corresponding to a diffuser of AR=3.

The circles depict the exit velocity distribution for the equivalent case of same Reynolds number and geometry configuration that was computed previously by solving the steady Navier-Stokes equations. Static pressure distribution evolution along the centerline in terms of a pressure coefficient $C_p$ is shown in Figure 45:
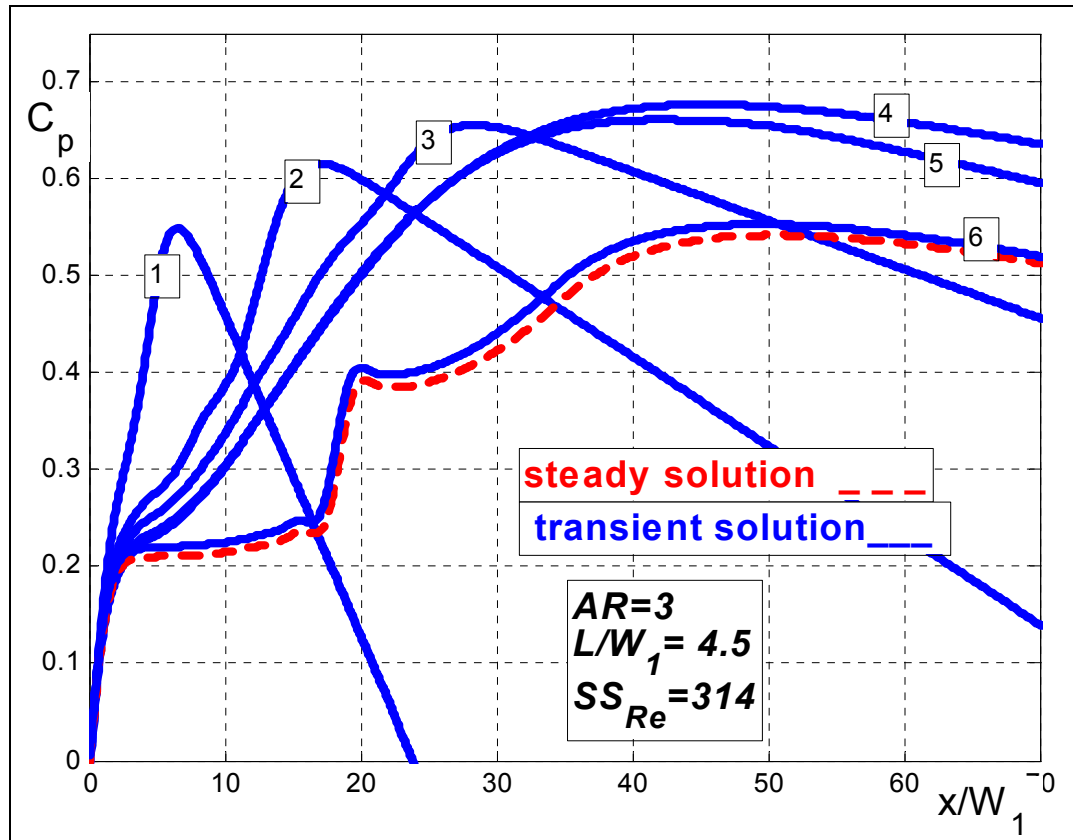


Figure 46.        Instantaneous pressure recovery curves.

It can be seen how the increasing influx of kinetic energy is converted to static pressure as the solution progresses in time. After sufficient amount of time the flow transitions from separated symmetric to separated asymmetric hence the drop in the overall pressure recovery. The red lines indicate the corresponding steady asymmetric solution found in the previous chapter for the same geometry and Re number. Numbers 1 through 6, indicate increasing time.

**2.      Flow Visualization**

Velocity and streamline contours evolving in time are given in Fig.45 for the examined cases below the lines (a-a) and (b-b). The flow starts impulsively and ends up to a steady asymmetric condition. It should be noted that before the asymmetric flow pattern is reached the flow temporarily passes through a symmetric separated condition and stays there for some milliseconds (time steps) before numerical truncation errors perturb the flow and drive it to the final more stable asymmetric configuration.
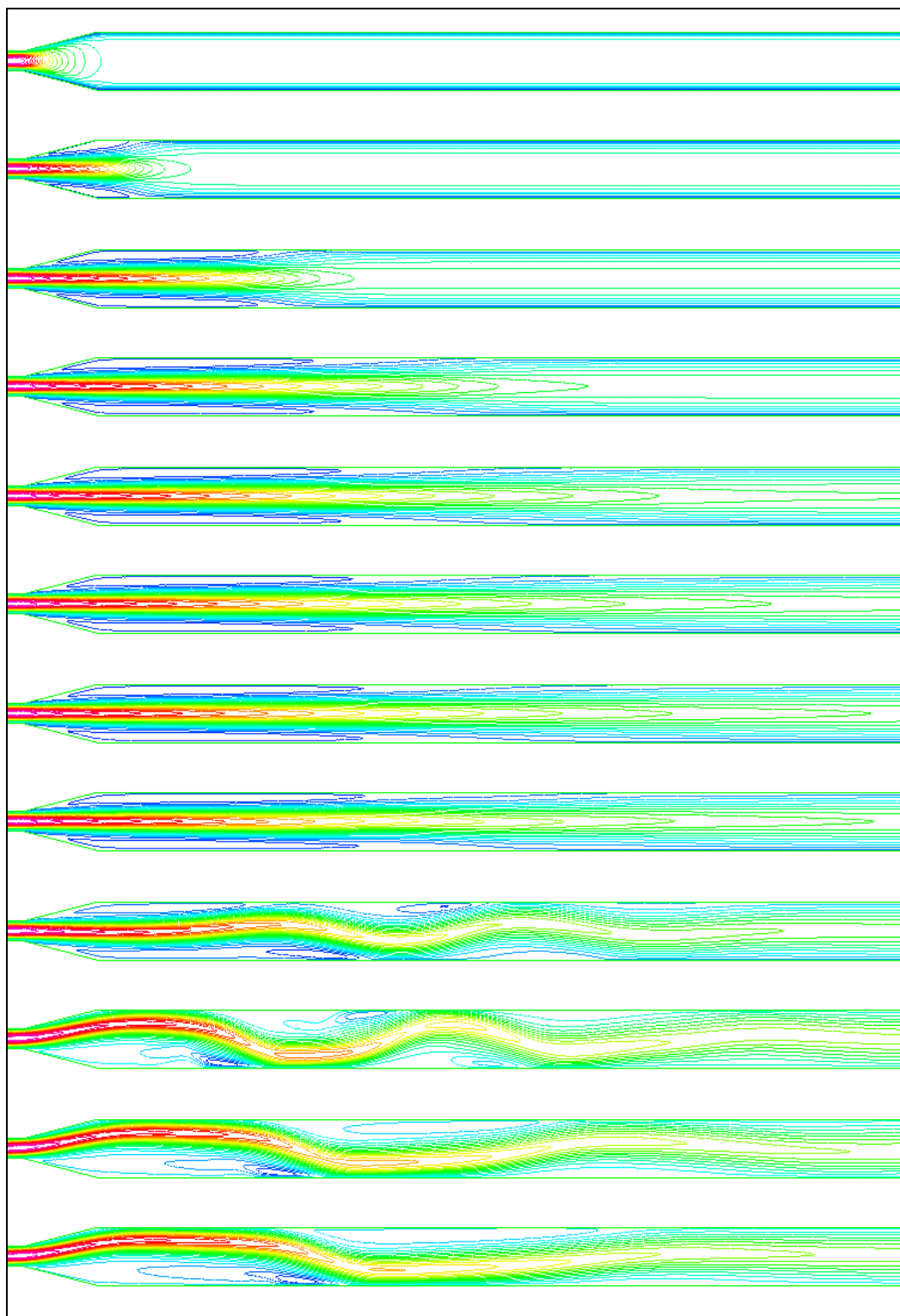
Figure 47.        Typical evolution of velocity contours in time for a case below the flow regime line b-b.
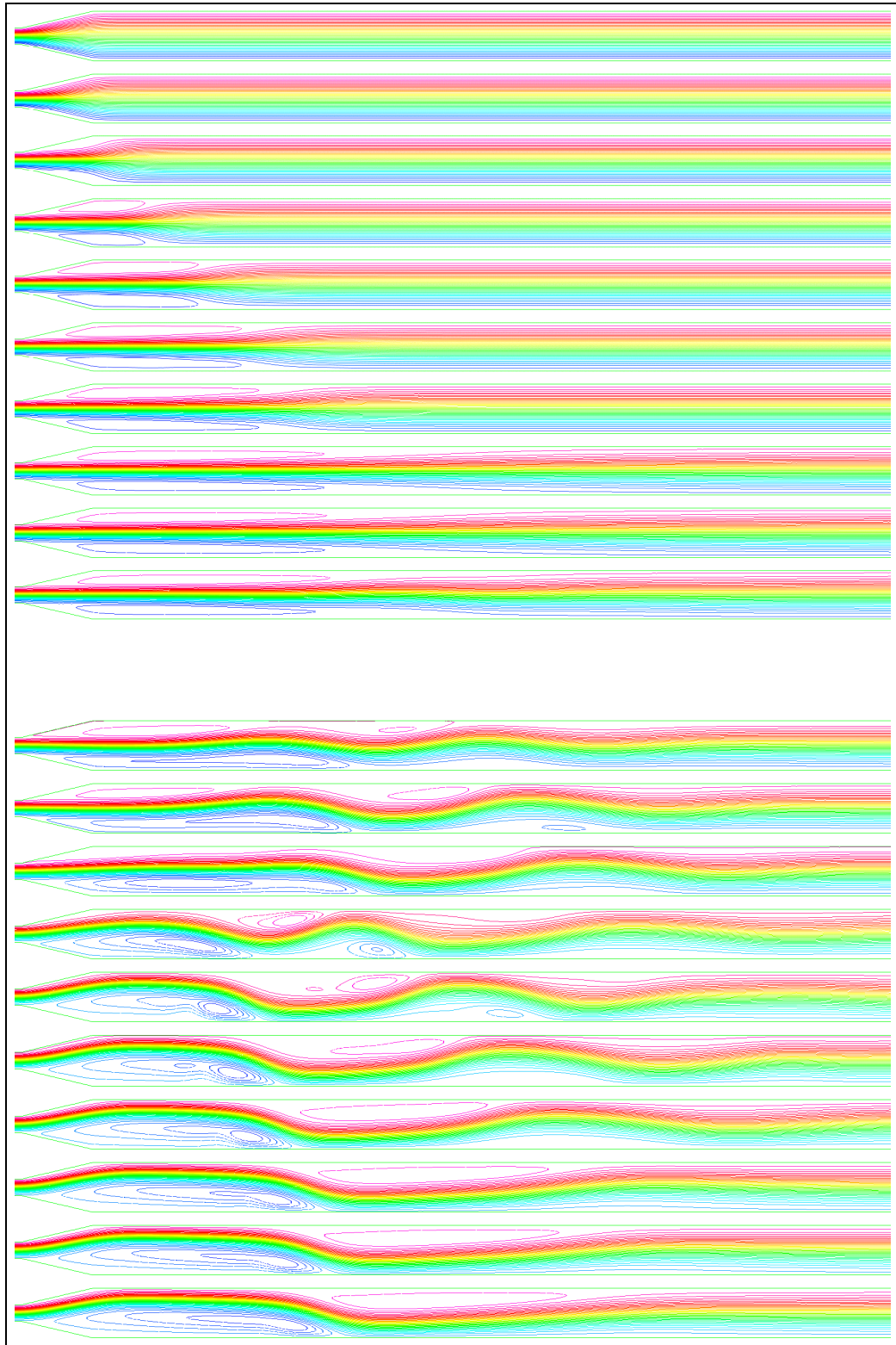
Figure 48.        Typical evolution of streamlines in time for case below the flow regime line

b-b.

For cases above lines a-a, b-b the flow starts impulsively and after sufficient time it does not approach a steady condition. On the contrary the flow develops initially as separated symmetric but after some time it has been found to break down shedding vortices in the downstream channel. Eventually these unsteady flow structures reach the boundaries where they no longer can be handled computationally because the boundaries downstream and upstream are invariant with time. Thus the solution accuracy in such cases is lost a few time steps beyond the onset of flow "break down". Nevertheless it is indicated that for cases above the lines a-a, b-b the flow seizes to be two-dimensional. It is believed that the flow becomes three-dimensional and unsteady in the regime above the lines given in Fig.29. The following Figure 49 shows velocity contour snap shots of successive time steps of such a case.
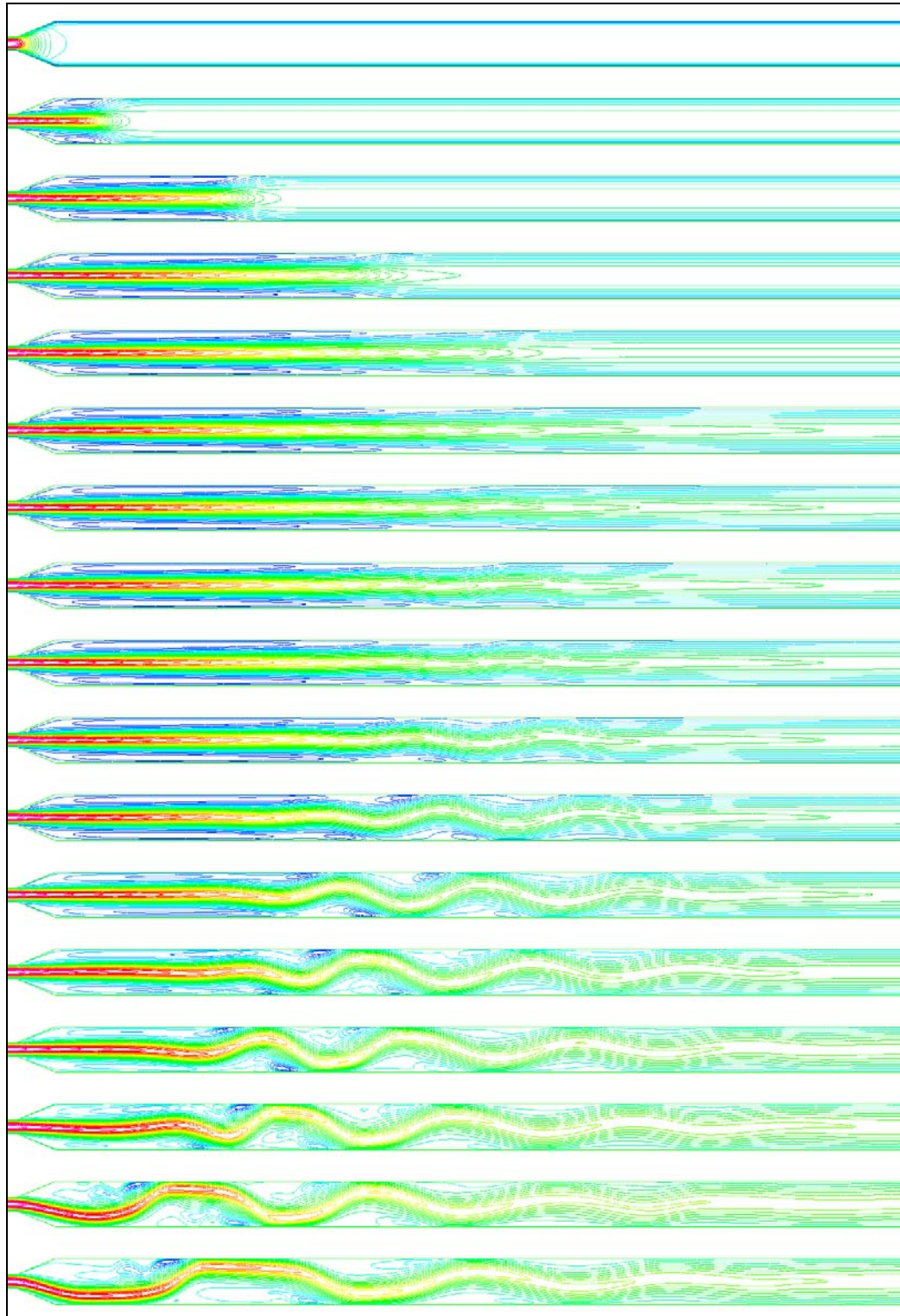
Figure 49. Typical evolution of velocity contours in time for case above the flow regime line b-b

THIS PAGE INTENTIONALLY LEFT BLANK

# VI. CONCLUSIONS

A commercial code was validated against the analytical solution of Jeffery-Hamel flows through two-dimensional diffusers with less than 1% error. The code was found very robust and user friendly and was used with a great degree of confidence for the subsequent computations of diffuser flow regime and performance maps. A large number of diffuser geometries (area ratios AR 1.15-5 and lengths over inlet height $L/W_1$ 1-48) were considered to compute flow regime and pressure recovery maps for incompressible laminar flow through 2-D plane diffusers by purely computational means in the Re range 105-1048.

A threshold combination of AR-$L/W_1$-Re exists beyond that the flow seizes to be steady two-dimensional. For AR-$L/W_1$-Re combinations were the flow remains two-dimensional both symmetric and asymmetric solutions of the equations are possible. The general trend is that increasing the divergence angle of diffuser, the pattern of the flow changes from attached to separated symmetric to separated asymmetric and finally to a non two-dimensional configuration.

Performance and flow regimes are a function of diffuser geometric parameters and Reynolds number. While Reynolds number increases (from 105 to 629) maximum pressure recovery exists for decreasing diffusion half angles (from ~12 degrees to ~ 3 degrees) and always in the two-dimensional flow regime.

The performance maps show that using a diffuser to connect two channels of different heights can be advantageous compared to having a sudden expansion. In addition the optimum region on the maps shifts to lower angles and higher diffuser lengths as Reynolds number increases. Limitations on the complete construction of the maps are imposed in this study by the fact that numerical calculations are possible only when the flow is two-dimensional (i.e. the program converges).

THIS PAGE INTENTIONALLY LEFT BLANK

# APPENDIX A. MATLAB CODE ON THE SOLUTION OF JEFFERY-HAMEL DIFFUSER FLOW NON-LINEAR ODE .

```
clear
global Re_r a
Re_r=1400;      % reduced Re number : Re_r=(a*Re), Re=?*V*r/?
a=2*5*pi/360;   % difffuser/Nozzle half angle(use + for diff. & - for nozz.)
%
A=linspace(0,1,1000);
x=-85.0484725; % initial curvature
[T,Y] = ode45(@hamel_1,[A],[1 0 x]);

figure(1)       % plot of the nondimensional vel. profiles in polar coord.
plot(T,Y(:,1),-T,Y(:,1))
grid on

%%%%%%%%%%%%%%%%%%%%%%%%%%%%%%%%%%%%%%%%%%%%%%%%%%%%%%%%
%    x VALUES (INITIAL CURVATURES) FOR THE SHOOTING
%    TO CONVERGE QUICKLY AND ACCURATELY:
%
%---Re*a--##------DIFFUSER-------##--------NOZZLE-----
%   0     ##    x=-2.00508465    ##    x=-2.00508465
%   50    ##    x=-3.5394176     ##    x=-1.121980
%   100   ##    x=-5.8691811     ##    x=-0.640165
%   118   ##    x=-6.8802251     ##    x=-0.526902
%   300   ##    x=-18.9682230    ##    x=-0.0912577
%   500   ##    x=-32.4654512    ##    x=-0.018555
%   800   ##    x=-52.3003336    ##    x=-0.0025015
%   1400  ##    x=-85.0484725    ##    x=-0.0000955
```

```
function dy=hamel_1(t,y)
global Re_r a
dy=zeros(3,1);
dy(1)=y(2);
dy(2)=y(3);
dy(3)= - 4.*a.^2.*y(2) -2.*a.*Re_r.* y(1).*y(2);
return
```

THIS PAGE INTENTIONALLY LEFT BLANK

# APPENDIX B. SELF-SIMILAR FLOWS IN CONICAL DIFFUSERS.

Assuming purely radial flow the velocity components are:

$$u_r = \frac{\nu F(\theta, \phi)}{r^2}, \qquad u_\theta = 0, \qquad u_\phi = 0$$

Substituting in the momentum equations we get:

r-momentum

$$u_r \frac{\partial u_r}{\partial r} + \frac{u_\theta}{r} \frac{\partial u_r}{\partial \theta} + \frac{u_\phi}{r \sin \theta} \frac{\partial u_r}{\partial \phi} - \frac{u_\theta^2 + u_\phi^2}{r} = -\frac{1}{\rho} \frac{\partial p}{\partial r} + \nu \nabla^2 u_r \Rightarrow \tag{37}$$

$$-\frac{2\nu^2 F^2}{r^5} = -\frac{1}{\rho} \frac{\partial p}{\partial r} + \frac{\nu^2}{r^4} \left( \frac{\partial^2 F}{\partial \theta^2} + \frac{1}{\sin^2 \theta} \frac{\partial^2 F}{\partial \phi^2} + \frac{\cos \theta}{\sin \theta} \frac{\partial F}{\partial \theta} \right) \tag{38}$$

θ-momentum

$$0 = -\frac{1}{r\rho} \frac{\partial p}{\partial \theta} + \frac{2\nu}{r^2} \frac{\partial u_r}{\partial \theta} \Rightarrow \tag{39}$$

$$\frac{\partial p}{\partial \theta} = \frac{2\rho \nu^2}{r^3} \frac{\partial F}{\partial \theta} \tag{40}$$

Φ-momentum

$$0 = -\frac{1}{r\rho \sin \theta} \frac{\partial p}{\partial \phi} + \frac{2\nu}{r^2 \sin^2 \theta} \frac{\partial u_r}{\partial \phi} \Rightarrow \tag{41}$$

$$\frac{\partial p}{\partial \phi} = \frac{2\rho \nu^2}{r^3 \sin \theta} \frac{\partial F}{\partial \phi} \tag{42}$$

Take the derivative of (38) with respect of θ, φ respectively and substitute the pressure gradient from (40) and (42) to get (44) and (46) respectively:

$$\frac{\partial}{\partial \theta}\left[-\frac{2\nu^2 F^2}{r^5}\right]=-\frac{1}{\rho}\frac{\partial}{\partial r}\left(\frac{\partial p}{\partial \theta}\right)+\frac{\partial}{\partial \theta}\left[\frac{\nu^2}{r^4}\left(\frac{\partial^2 F}{\partial \theta^2}+\frac{1}{\sin^2\theta}\frac{\partial^2 F}{\partial \phi^2}+\frac{\cos\theta}{\sin\theta}\frac{\partial F}{\partial \theta}\right)\right]\Rightarrow \quad (43)$$

$$-\frac{4}{r}F\frac{\partial F}{\partial \theta}=6\frac{\partial F}{\partial \theta}+\frac{\partial^3 F}{\partial \theta^3}+\frac{1}{\sin^2\theta}\frac{\partial^3 F}{\partial \phi^2\,\partial \theta}+\frac{\cos\theta}{\sin\theta}\frac{\partial^2 F}{\partial \theta^2}-\frac{2\cos\theta}{\sin^3\theta}\frac{\partial^2 F}{\partial \phi^2}-\frac{1}{\sin^2\theta}\frac{\partial F}{\partial \theta} \quad (44)$$

And,

$$\frac{\partial}{\partial \phi}\left[-\frac{2\nu^2 F^2}{r^5}\right]=-\frac{1}{\rho}\frac{\partial}{\partial r}\left(\frac{\partial p}{\partial \phi}\right)+\frac{\partial}{\partial \phi}\left[\frac{\nu^2}{r^4}\left(\frac{\partial^2 F}{\partial \theta^2}+\frac{1}{\sin^2\theta}\frac{\partial^2 F}{\partial \phi^2}+\frac{\cos\theta}{\sin\theta}\frac{\partial F}{\partial \theta}\right)\right] \quad (45)$$

$$-\frac{4}{r}F\frac{\partial F}{\partial \phi}=\frac{6}{\sin\theta}\frac{\partial F}{\partial \theta}+\frac{\partial^3 F}{\partial \theta^2\,\partial \phi}+\frac{1}{\sin^2\theta}\frac{\partial^3 F}{\partial \phi^3}+\frac{\cos\theta}{\sin\theta}\frac{\partial^2 F}{\partial \theta\,\partial \phi} \quad (46)$$

Equations (44) and (46) form a system that must be solved to get the velocity profiles $F(\theta,\phi)$. However r remains a parameter in the equations thus there is no unique solution independent of r. For instance a symmetric with respect to r bell shaped velocity profile has $\partial F/\partial \phi=0$. Equation (46) is satisfied and equation (44) becomes an ODE where r is a parameter again:

$$-\frac{4}{r}F\frac{dF}{d\theta}=6\frac{dF}{d\theta}+\frac{d^3 F}{d\theta^3}+\frac{\cos\theta}{\sin\theta}\frac{d^2 F}{d\theta^2}-\frac{1}{\sin^2\theta}\frac{dF}{d\theta}$$

Thus for point source flows through conical diffuser there exists no similarity solution.

# APPENDIX C. SUDDEN EXPANSION FLOW COMPUTATIONS

## A.    INVISCID STREAMLINE SLOPE COMPUTATIONS

```
%
u=ones(100,100);   % initial guess
v1=100;            % inlet velocity (m/sec)
rho=1.2;           % density (Kg/m3)
p1=100e3;          % inlet pressure (Pa)
[m,n]=size(u);
% boundary conditions
  % upper boundary
  u( 1  , 1:50 ) = 50;
  u(1:81, 50   ) = 50;
  u( 81 , 51:100) = 50;
  % lower boundary
  u( 100,1:100   ) = 0;
  % inlet
  u( :  , 1 )  = flipud(linspace(0,50,100)');
  % outlet
  u(81:100,100) = flipud(linspace(0,50,20)');
%
for niter=1:1200 % # of iterations
   for j=2:n-51
    for i=2:m-19
        u(i,j)=.25*( u(i,j+1) + u(i,j-1) + ...
                     u(i+1,j) + u(i-1,j));
    end
   end

   for j=2:n-1
    for i=82:m-1
        u(i,j)=.25*( u(i,j+1) + u(i,j-1) + ...
                     u(i+1,j) + u(i-1,j));
    end
   end
end
%
```

```
%
figure (1)
 u(1:80,51:100)=NaN;
 phsi=[u(1:99,:);flipud(u(1:100,:))]; % stream function values
 contour(phsi,60) % plot of stream function inside the contraction
 title(' Stream lines ')
 axis off

% : % difference of stream function values
parall_diff1=100*norm(u(:,1)-u(:,2))
parall_diff2=100*norm(u(81:100,75)-u(81:100,100))
```



Stream lines

AR=5
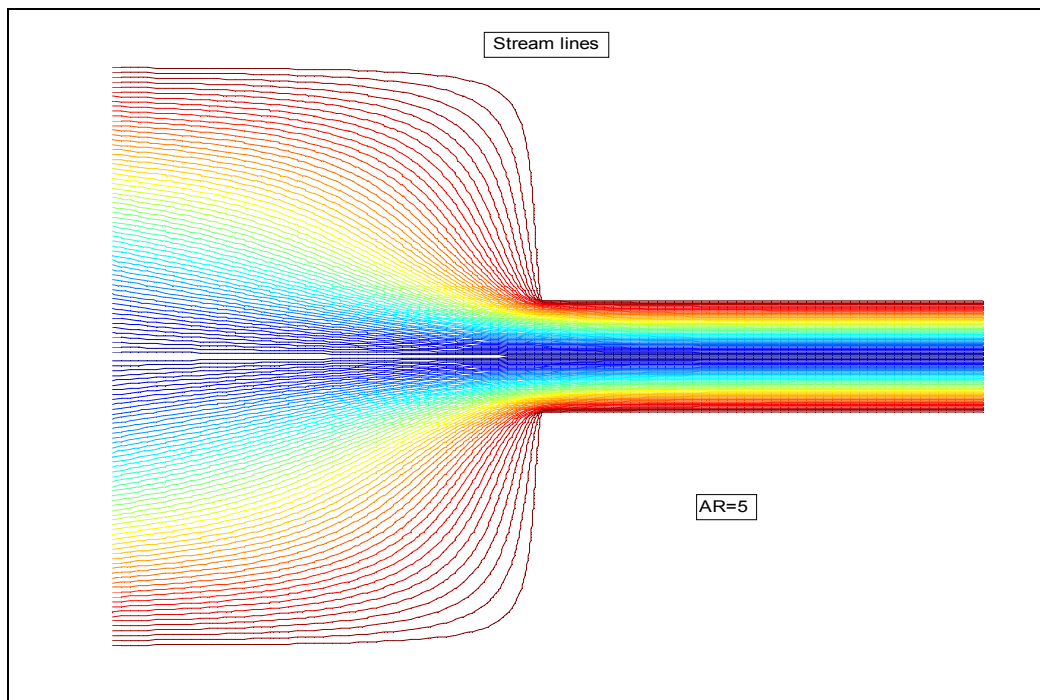
## B.    PSEUDO-INVISCID PRESSURE RECOVERY FOR A SUDDEN EXPANSION

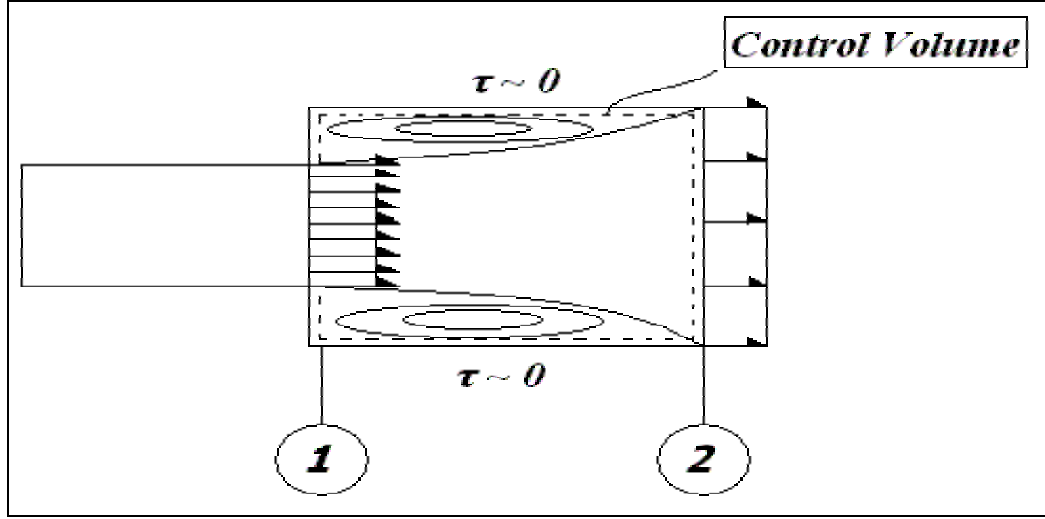For incompressible flow the sum of the forces on the control volume indicated in Fig.49 reads:



Figure 50.       Expansion flow schematic.

$$p_1 A_1 - p_2 A_2 + \tau A_{sides} = (\rho A_2 U_2)U_2 - (\rho A_1 U_1)U_1 \qquad (47)$$

Where p, U, A are static pressures, velocities, areas at stations 1, 2 respectively. It is reasonable to assume that the pressure at station 1 is applied to the whole face area at station 1 i.e. $A_1 = A_2$. Then using continuity $U_1 A_1 = U_2 A_2$ to eliminate velocities and dividing by the dynamic head at station 1, equation (23) becomes:

$$C_p = \frac{p_2 - p_1}{0.5\rho U_1^2} = \frac{2A_1}{A_2}\left[1 - \frac{A_1}{A_2}\right] \qquad (48)$$

Where $C_p$ is the coefficient of pressure recovery. The total pressure loss coefficient $C_{pT}$ for the same expansion flow configuration reads:

$$C_{pT} = \frac{P_{T1} - P_{T2}}{0.5\rho U_1^2} = \left[1 - \frac{A_1}{A_2}\right]^2 \qquad (49)$$

Where $P_T$ denotes total pressures. For potential flow through the expansion the ideal recovery is:

$$C_{p,i} = 1 - \frac{1}{\left( \frac{A_2}{A_1} \right)^2} \qquad (50)$$

Equations 24, 25, 26 are plotted together in Fig.50. An area ratio of 2 gives the max recovery of 0.5.

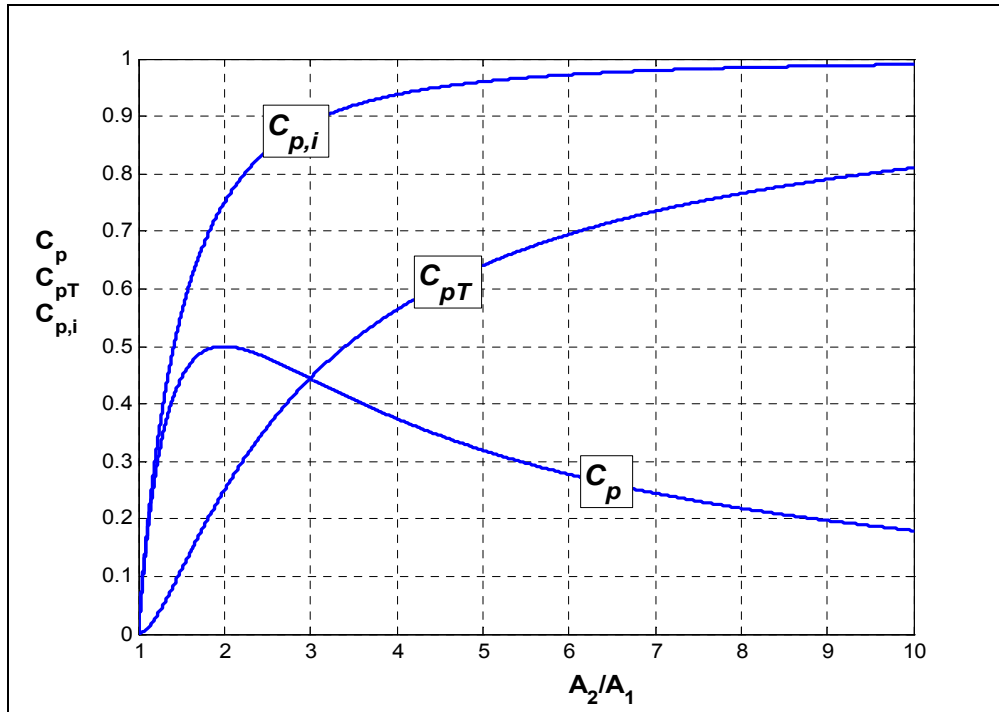

Figure 51.       Pressure recoveries $C_p$, $C_{pT}$, $C_{p,i}$.

# APPENDIX D. FLOW REGIME MAP EXTRACTION METHOD FROM THE NUMERICAL DATA

The following figures show the actual numerical data from which the interpolating lines of Figure 29 are drawn. Power laws of the form (51) interpolate the numerical data points at the uppermost corners of the poly-lines shown in figures in order to construct the flow regime map:

$$AR = e^b \left( \frac{L}{W_1} \right)^a \tag{51}$$

For each flow regime line the exponents a, b are shown in Table 4 below:

Table 4    Flow regime map line exponents.

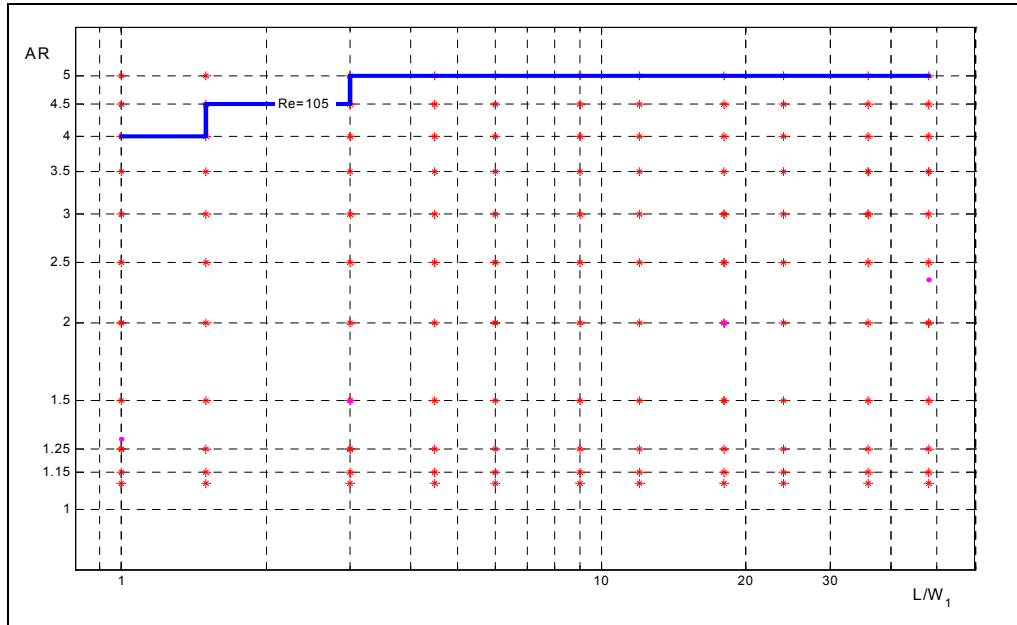| Re | a | b |
|---|---|---|
| 105 | 0.1976 | 1.4009 |
| 210 | 0.2479 | 1.1688 |
| 314 | 0.2261 | 0.8350 |
| 420 | 0.1878 | 0.5956 |
| 629 | 0.1773 | 0.4399 |
| 1048 | 0.1626 | 0.2245 |



Figure 52.        Flow regime map data for Re=105.
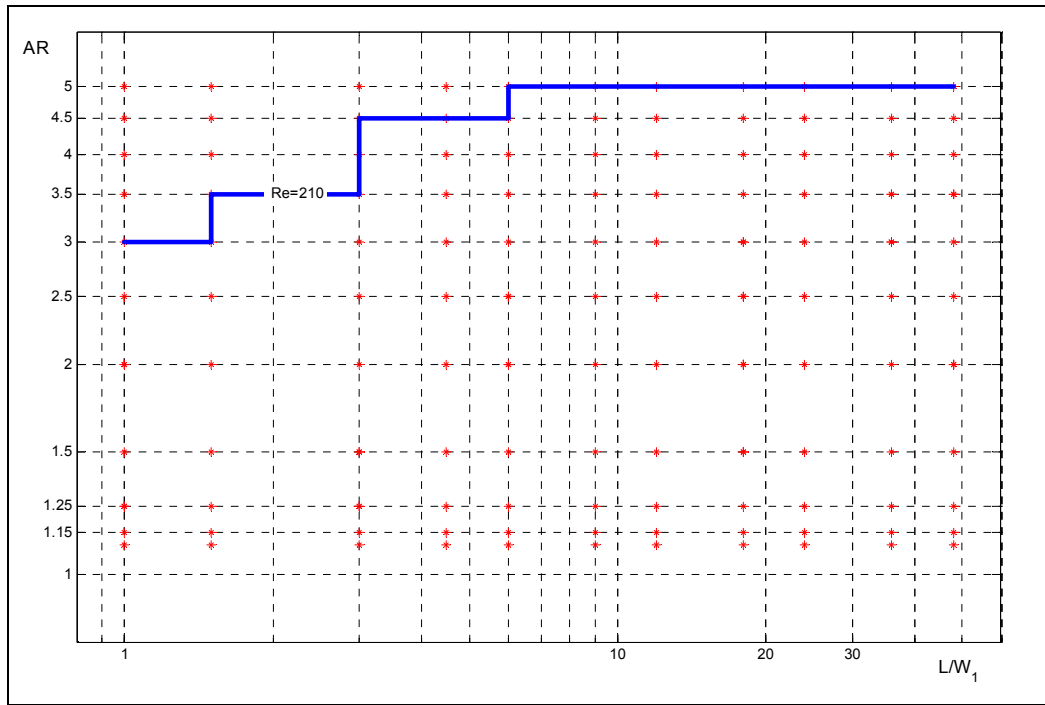
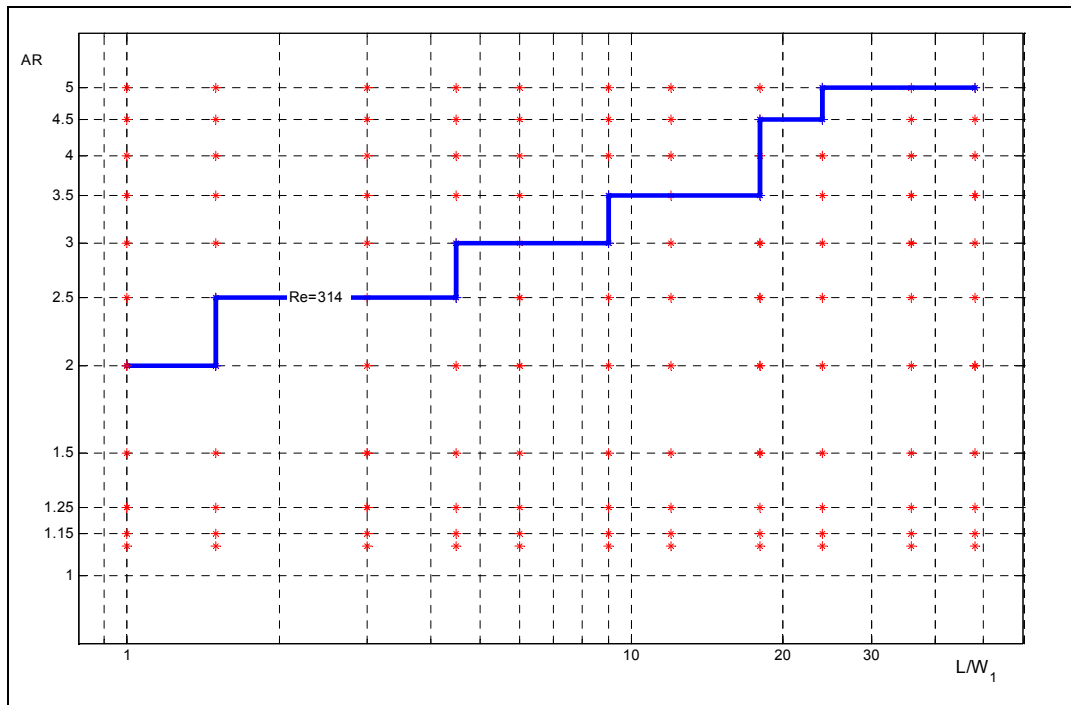Figure 53.        Flow regime map data for Re=210.



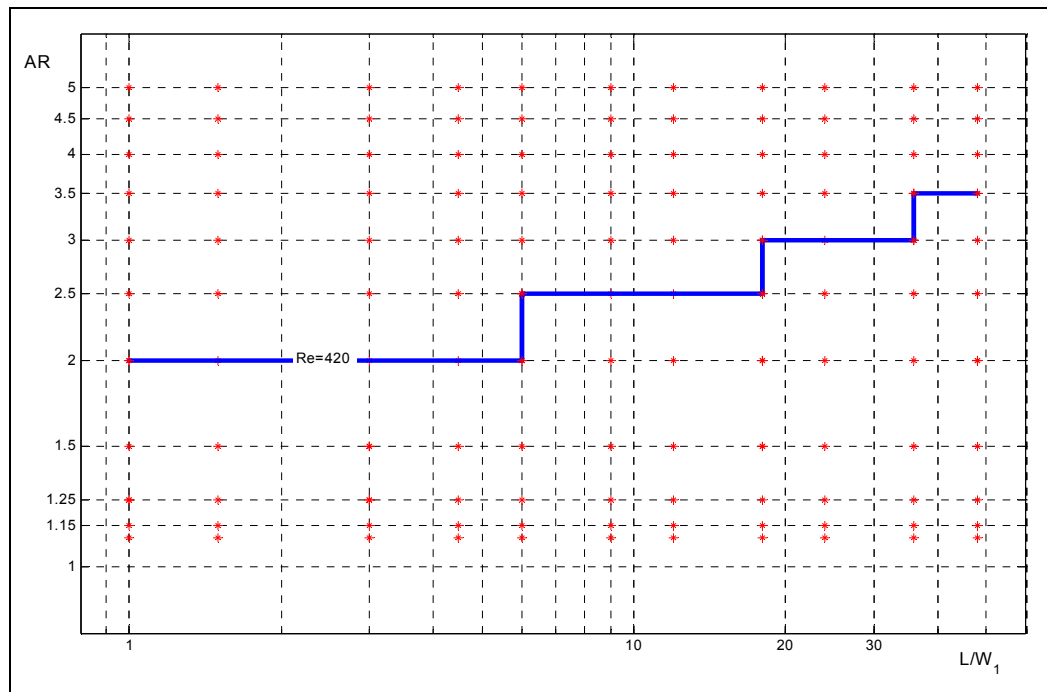Figure 54.        Flow regime map data for Re=314.

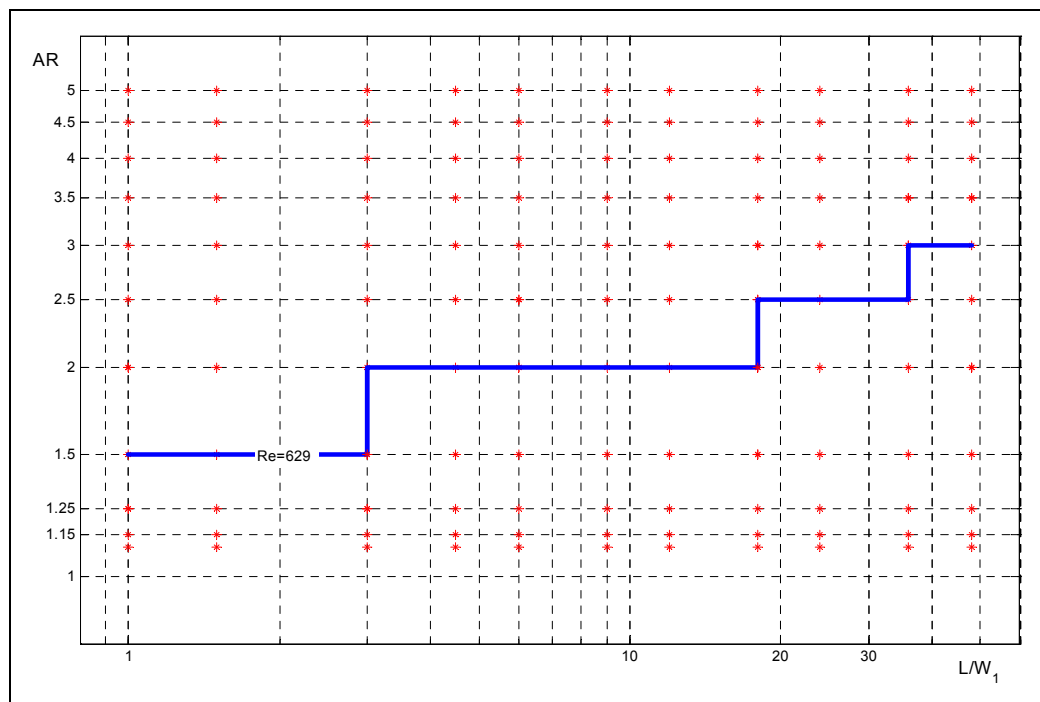Figure 55.        Flow regime map data for Re=420



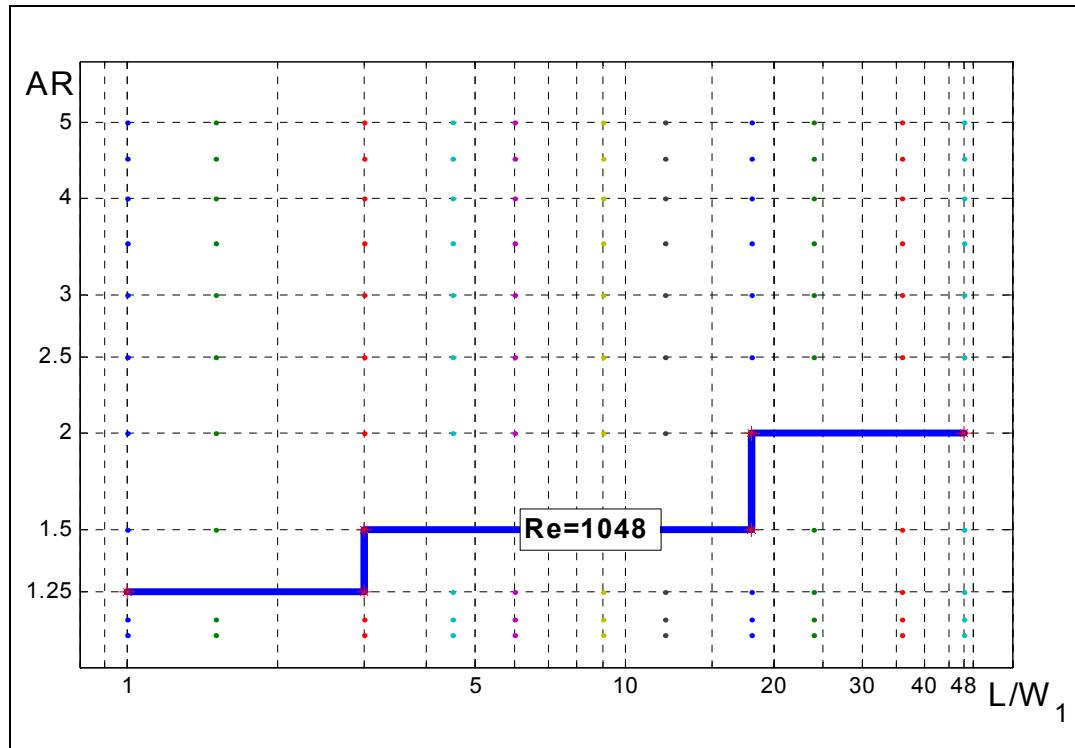Figure 56.        Flow regime map data for Re=629.

73

Figure 57.      Flow regime map data for Re=1048.

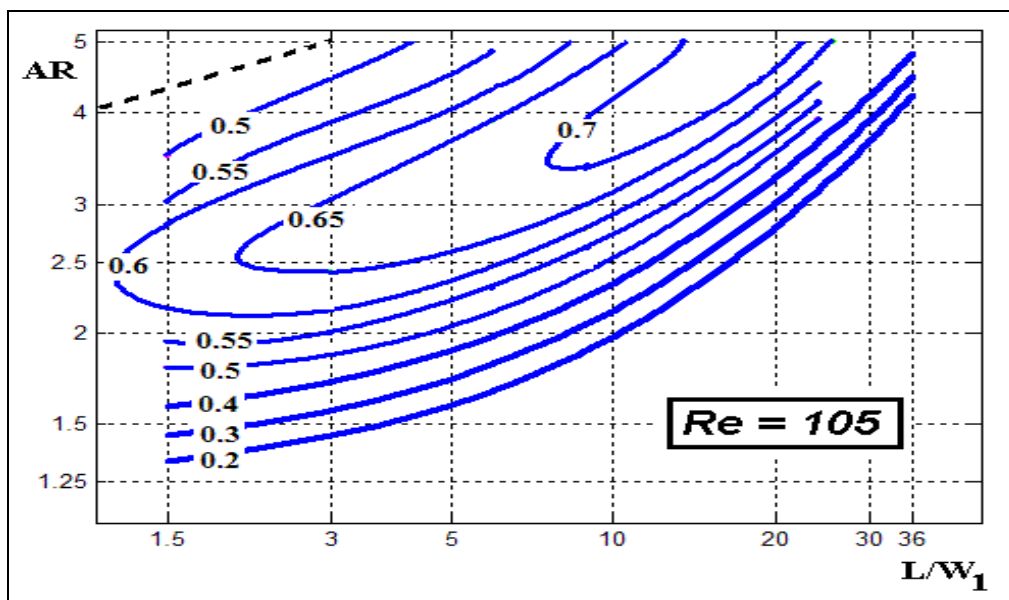## APPENDIX E. DIFFUSER PERFORMANCE MAPS FOR REYNOLDS NUMBERS OF 105, 210, 314, 420 AND 629



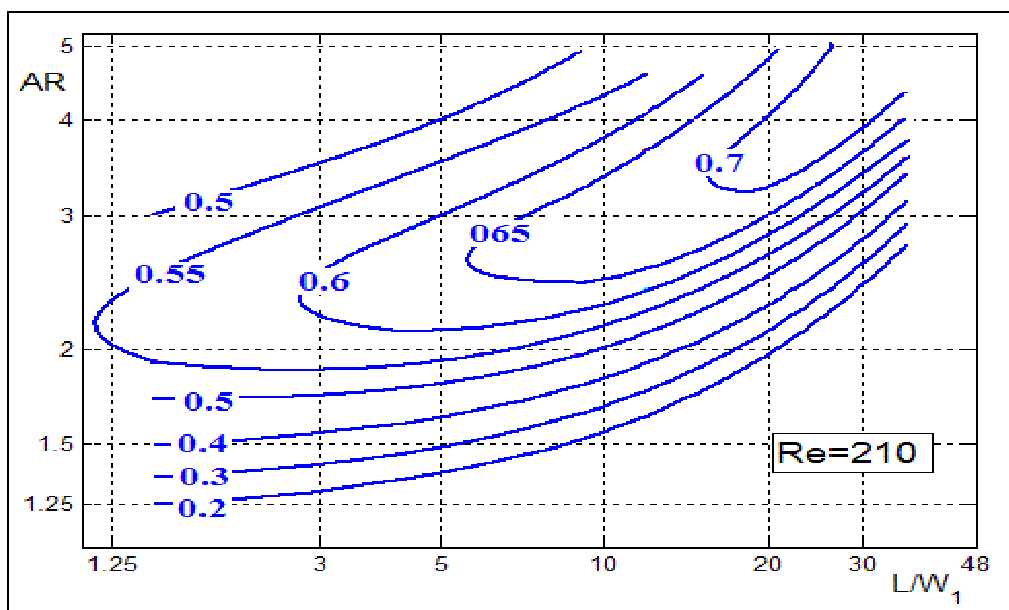Figure 58.      Diffuser performance map for Re=629 with the respective asymmetric flow regime line.



Figure 59.      Diffuser performance map for Re=629 with the respective asymmetric flow regime line.
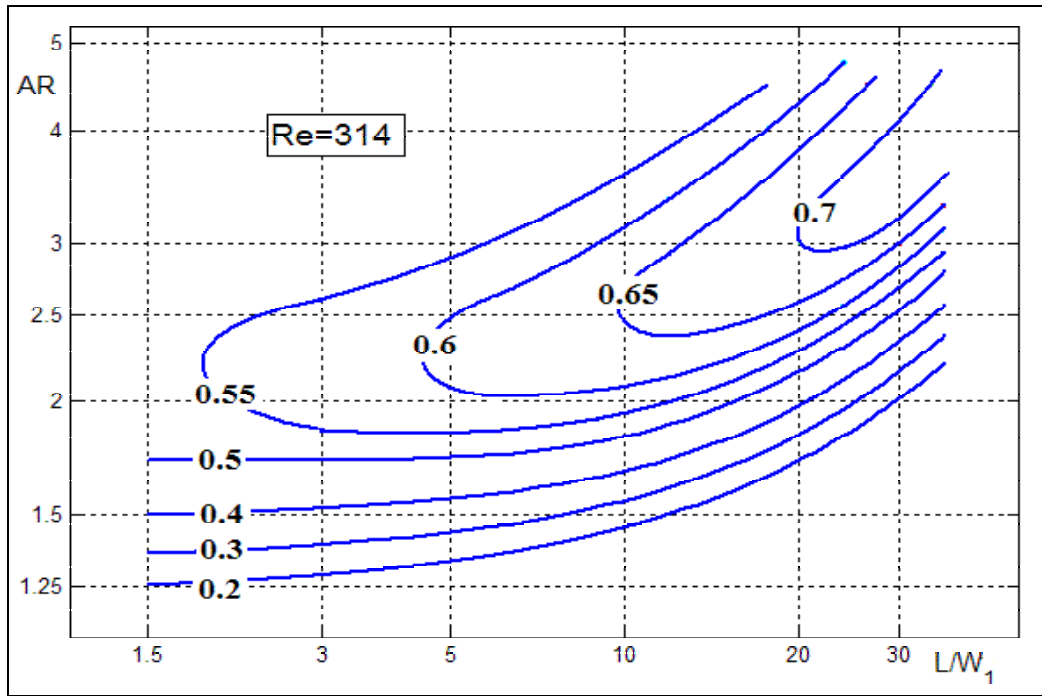
Figure 60.        Diffuser performance map for Re=629 with the respective asymmetric flow
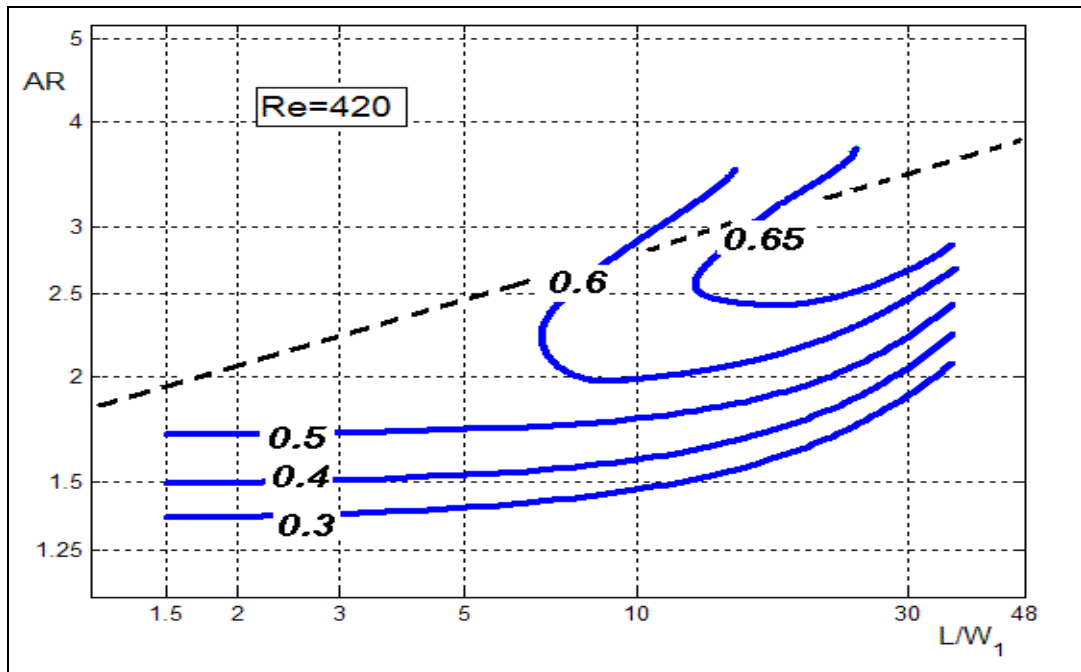regime line.



Figure 61.        Diffuser performance map for Re=420 with the respective asymmetric flow
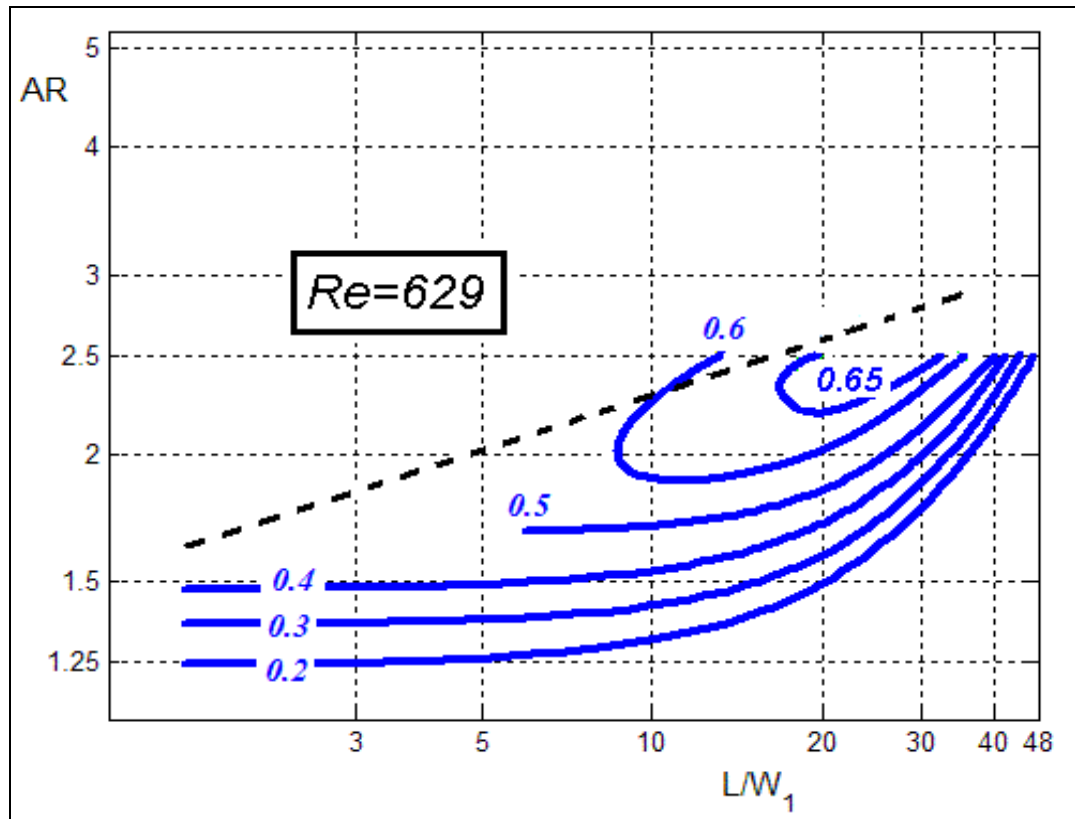regime line.

Figure 62.    Diffuser performance map for Re=629 with the respective asymmetric flow regime line.

THIS PAGE INTENTIONALLY LEFT BLANK

# LIST OF REFERENCES

1.  S.J. Kline, D.E.Abbott, R.W. Fox, "Optimum design of straight-walled diffusers", J. Basic Eng., Sept. 1959, pp321-331.

2.  B.A. Waitman, L.R. Reneau, S.J. Kline"Effects of inlet conditions on performance of two dimensional subsonic diffusers", J. Basic Eng, Sept. 1961, pp349-360.

3.  G.Sorvan, E.D. Klomp, "Experimentally determined optimum geometries for rectilinear diffusers with rectangular, conical or annular cross-sections", Fluid mechanics of internal flow, Elsevier Publishing Co., New York, 1967pp270-319.

4.  L.R. Reneau, J.P. Johnston, S.J.Kline, "Performance and design of straight, two dimensional diffusers" J. Basic Eng., Mar. 1967, pp141-150.

5.  S. Wolf, J.P. Johnston, "Effects of non-uniform inlet velocity profiles on flow regimes and performance in two-dimensional diffusers." JBE, Sept. 1969, pp462-474.

6.  O.J. McMillan, J.P. Johnston,"Performance of low-aspect ratio diffusers with fully developed turbulent inlet flows.", Part I, J. Fluids Eng., Sept. 1973, pp385-400.

7.  O.J. McMillan, J.P. Johnston, "Performance of low-aspect ratio diffusers with fully developed turbulent inlet flows.", Part II, J. Fluids Eng., Sept. 1973, pp385-400.

8.  P.W. Runstadler Jr, F.X. Dolan, " Data on pressure recovery performance of straight-channel, plane divergence diffusers at high subsonic mach numbers", J. Fluids Eng., Sept. 1973, pp373-384.

9.  P.W. Runstadler Jr, F.X.Dolan, "Pressure recovery performance of conical diffusers at high subsonic mach numbers", NASA report CR-2299.

10. A.S. Dighe, A.T. McDonald, "Effects of aspect ratio and low Reynolds number on recovery and flow regimes in a plane-wall diffuser." Symposium on fluidic-state-of-the-art, (1974 Washington D.C.)

11. A.H. Stenning,A.A.Schachenmann,"Oscillatory flow phenomena in diffusers at low Reynolds numbers", J. Fluids Eng., Sept. 1973, pp401-407.

12. C.R. Smith,Jr., S.J. Kline, " An experimental investigation of the transitory stall regime in two-dimensional diffusers", J. Fluids Eng., Mar. 1974, pp.11-15.

13. A.H.M. Kwong, A.P. Dowling, " Unsteady flow in diffusers", J. Fluids Eng., Dec. 1994, pp842-847.

14. Y. Senoo, M. Nishi, "Improvement of the performance of Diffusers by Vortex generators", J. Fluids Eng., Mar. 1974, pp4-10.

15. A.H.M. Kwong, A. P. Dowling, "Active Boundary layer control in diffusers" AIAA Journal, Dec. 1994.

16. A.J. Ward-Smith, D.L. Lane, A. J. Reynolds, B. Sahin, D.J. Shawe, " Flow regimes in wide-angle screened diffusers", International J. Mechanical Sciences Vol 33, No1, pp41-54, 1991.

17. Y. G. Lai, R.M. So, B.C. Hwang, "Calculation of planar and conical diffuser flows", AIAA Journal, Vol. 27, 1987, pp542-548.

18. Yeng-Y. Tsui, Chia-K. Wang, "Calculation of Separated flow in Symmetric two-dimensional diffusers", J. Fluids Eng., Dec. 1995 pp612-616.

19. D.Xu B.C. Khoo, M.A. Leschziner "Numerical simulation of turbulent flow in an axisymetric diffuser with a curved surface center-body", International J. of Numerical Methods for Heat & Fluid flow, Vol.2 1998 pp245-255.

20. S. Chakrabarti, S. Ray, A. Sarkar, "Numerical simulation of the performance of a vortex controlled diffuser in low Reynolds number regime", International J. of Numerical Methods for Heat & Fluid flow, Vol.12 2002 pp224-240.

21. K. Millsaps, K. Pohlhausen, "Thermal distributions in Jeffery-Hamel flows between non-parallel plane walls" J. Aeronautical Sciences, Mar. 1953 pp187-196.

22. CFD-ACE+ user Manual.

23. F. M. White, Viscous Fluid Flow, 2d ed., McGraw-Hill, New York, 1991.

24. G. K. Batchelor, An Introduction to Fluid Dynamics, Cambridge University Press, Cambridge, England, 1967.

# INITIAL DISTRIBUTION LIST

1.  Dudley Knox Library
    Naval Postgraduate School
    Monterey, California

2.  Professor Knox T. Millsaps Jr., Code ME/MI
    Department of Mechanical Engineering
    Naval Postgraduate School
    Monterey, California